Evaluation of Northern Hemisphere blocking climatology in the Global Environment Multiscale (GEM) model

Etienne Dunn-Sigouin , Seok-Woo Son *

Department of Atmospheric and Oceanic Sciences, McGill University, Montréal, Québec, Canada

Hai Lin

Atmospheric Numerical Weather Prediction Research, Environment Canada, Dorval, Québec, Canada

* *Corresponding author address:* Seok-Woo Son, McGill University, 805 rue Sherbrooke Ouest, Montreal, QC H3A2K6.

E-mail: seok-woo.son@mcgill.ca

ABSTRACT

The performance of the Global Environmental Multiscale (GEM) model, the Canadian operational numerical model, in reproducing atmospheric low-frequency variability is evaluated in the context of Northern Hemisphere blocking climatology. The validation is conducted by applying a comprehensive but relatively simple blocking detection algorithm to a 20-year (1987-2006) integration of the GEM model in climate mode. The comparison to reanalysis reveals that, although the model can reproduce Northern Hemisphere blocking climatology reasonably well, the maximum blocking frequency over the north Atlantic and western Europe is generally underestimated and its peak season is delayed from late winter to spring. This contrasts with the blocking frequency over the north Pacific which is generally overestimated during all seasons. These misrepresentations of blocking climatology are found to be largely associated with the biases in climatological background flow. The modelled stationary waves show a seasonal delay in zonal wavenumber 1 and an eastward extension in zonal wavenumber 2 components consistent with blocking frequency biases. High-frequency eddies are, however, consistently underestimated both in the north Atlantic and Pacific, indicating that the biases in eddy fields might not be the main reason for the blocking biases in the north Pacific.

1. Introduction

Atmospheric blocking is one of the most striking features of extratropical low-frequency variability. A synoptic-scale high pressure system, often accompanied by low pressure system at lower latitudes, occasionally becomes quasi-stationary for several days to a few weeks against the background flow. This quasi-stationary system, referred to as a block, interrupts the eastward propagation of synoptic disturbances by reversing the climatological zonal flow.

As a blocking high is quasi-stationary by nature, it has a significant impact on surface weather and climate (e.g., Rex 1950; Trigo et al. 2004). A dramatic example is the 2010 Russian heat wave that resulted from a blocking episode that persisted for over a month (Dole et al. 2011). This event is associated with over 15,000 deaths in Russia and severe economic losses in neighbouring countries through crop damage (Matsueda 2011). The resulting downstream trough has also been suggested as a possible culprit of Pakistan flooding in 2010 (Webster et al. 2011).

The impact of blocking is not limited to the surrounding regions of a blocking high. It is known that long-lasting blocking events are often associated with extratropical teleconnection patterns (Renwick and Wallace 1996; Shabbar et al. 2001; Croci-Maspoli et al. 2007a; Woollings et al. 2008). In the Northern Hemisphere (NH), the preferred regions of blocking occurrence are the Europe-northeastern Atlantic (hereafter EA blocking) and the north Pacific (PA blocking), with a less frequent tertiary region over western Russia. The EA and PA blocking regions coincide with the preferable locations of two leading teleconnection patterns in the NH: namely the North Atlantic Oscillation (NAO) and the Pacific North American (PNA) pattern. It is hence not surprising to find that, EA blocking events are often concurrent with the negative phase of the NAO whereas PA blocking events are often associated with the negative phase of the PNA, although the causal relationship is unclear. Recent studies further showed that NH blocking events could even affect the stratospheric circulation. Martius et al. (2009) demonstrated that long-lasting blocks could excite planetary-scale waves that propagate into the stratosphere and break at the polar vortex

during the cold season, causing the so-called sudden stratospheric warming. Woollings et al. (2010) and Kolstad et al. (2010) proposed that there might be a two-way interaction between stratospheric circulation and tropospheric blockings.

The importance of blocking highs on local and remote weather systems has increased the need for the reliable simulation of blocking events in climate models. It is however known that blocking frequency is generally underestimated in the current generation of climate models (D'Andrea et al. 1998; Scaife et al. 2010). This failure has often been attributed to the model resolution (Tibaldi et al. 1997; Ringer et al. 2006; Matsueda et al. 2009). The poleward advection of anticyclonic vorticity and upscale entrophy cascade by high frequency transient eddies is widely recognized as an important mechanism for blocking maintenance (e.g., Shutts 1983; Mullen 1987; Nakamura et al. 1997). It follows that if high-frequency eddy activity is underestimated by model resolution, it could lead to rather weak eddy forcing and subsequently less frequent long-lived blocking events. This resolution issue is well documented for EA blockings (Tibaldi et al. 1997; Ringer et al. 2006; Matsueda et al. 2009). The corresponding effect on PA blockings, however, is not quite clear, suggesting that PA blocking is likely affected by other dynamical processes as well (Tibaldi et al. 1997). Matsueda et al. (2009) in fact showed that PA blocking could be significantly overestimated in high-resolution model simulations.

It is known that not only transient eddies but also the time-mean flow is important in simulating NH blockings. The influence of the time mean flow, especially the location of the westerly jet, on the formation of blocking was explicitly discussed in Kaas and Branstator (1993) who forced their GCM towards a zonal mean state representing suppressed or enhanced blocking activity. As anticipated, they found more frequent blocking events with the mean state associated with enhanced blocking activity, that is, relatively strong zonal winds around 30°N and weak winds around 50-60°N. In accordance with this finding, Barnes and Hartmann (2010) found a robust reduction in EA blocking frequency with the poleward shift of the Atlantic eddy-driven jet in Coupled Model Inter-comparison Project phase 3 (CMIP3)

scenario integrations.

In regards to the shape and intensity of the jet, it has been shown that excessive zonality and the underestimation of stationary wave could be an important source of error in blocking simulations (Doblas-Reyes et al. 2002; Barriopedro et al. 2010a). Excessive westerlies may result from anomalous momentum transfer from synoptic-scale eddies to the mean flow, decreasing the frequency of large-scale ridges over blocking regions (Wallace and Hsu 1985; Doblas-Reyes et al. 2002). In the diagnostic study by Cash and Lee (2000), linear interactions between low-frequency eddies and the time-mean flow are shown to dominate the vorticity budget during the onset and decay of modelled EA blocking. Their results suggest that systematic model biases in background flow could affect the role of those interactions by modifying the background potential vorticity gradient.

The importance of the background flow is further consistent with theoretical approaches that consider blocking as the result of wave-wave interactions such as the interference or resonant interaction of planetary-scale waves (e.g., Austin 1980; Colucci et al. 1981; Egger 1978) or the interaction of transient eddies and quasi-stationary planetary-scale waves (e.g., Colucci 1985; Nakamura et al. 1997; Cash and Lee 2000; Hu et al. 2008). It follows that weaker planetary-scale wave activity in the model could result in weaker interactions between waves, causing less frequent blocking events in the model (Doblas-Reyes et al. 2002; Barriopedro et al. 2010a).

The model biases in blocking climatology may result from multiple factors instead of any single factor. In fact it is often difficult to identify the exact reason of model biases as individual factors (e.g., high-frequency eddies, quasi-stationary waves, time-mean flow, etc.) are interacting with each other. The evaluation of numerical models in the context of blocking climatology is however still helpful for quantitative understanding of model performance and possible attribution of model biases. This is particularly true for operational models as blocking is one of the most important low-frequency variability in the extratropics which has a significant impact on surface weather.

Extending previous studies, the present study examines NH blocking climatology in an operational model. Specifically, the Canadian operational model, Global Environment Multiscale (GEM) model, is evaluated by applying a hybrid blocking index to the long-term model output. The blocking index employed in this study differs from traditional ones as it combines the two most commonly-used blocking indices. Since it combines advantages of the two indices, it is more comprehensive than each index but still relatively simple. This index is applied to both the reanalysis and model output to objectively characterize blocking climatology. The possible sources of blocking biases are then discussed by examining blocking statistics, stationary wave, transient eddies and energetics. Although this type of study, model validation in the context of blocking climatology, is not new, the identified blocking bias in the model turns out somewhat different from the one typically documented in the literature. It is found that blocking frequency over North Pacific is overestimated in most seasons even if the model is integrated with relatively coarse resolution. This contrasts with EA blocking whose frequency is either overestimated or underestimated depending on the season.

This paper is organized as follows. The data used in this study are briefly described in section 2. Section 3 presents the motivation and details of our blocking index. It is followed by 50-year climatology of the reanalysis data. The blocking simulated by the model is then evaluated in section 5 by comparing a 20-year blocking climatology with reanalysis data for the same time period. The possible sources of blocking biases are discussed in section 6 with an emphasis on the bias in time-mean flow.

2. Data

The reference blocking climatology is constructed from the National Centers for Environmental Prediction (NCEP)-National Center for Atmospheric Research (NCAR) Reanalysis data (NNR, Kalnay et al. (1996)). The 50-year long data, from 1960 to 2009, are used to

generate a long-term climatology, and to validate the blocking index employed in this study.

The model evaluated in this study is the GEM model of Recherche en Prévision Numérique, Environment Canada (Côte et al. 1998a,b). It is an operational forecast model at the Canadian Meteorological Centre, and is integrated in climate mode by using the version 3.2.2 at a horizontal resolution of 2° latitude by 2° longitude with 50 vertical levels (the model top at 5 hPa). The model was initialized at 00Z of January 1, 1985, and integrated for 22 years by prescribing surface boundary conditions from the Seasonal prediction Model Intercomparison Project-2 (SMIP-2) boundary data. After discarding first two years of spin-up period, 20 years of data, from 1987 to 2006, are analyzed. All daily mean data are first interpolated into 2.5° latitude by 2.5° longitude resolution to be consistent with the NNR resolution. Blocking statistics and the related analyses are then performed using this interpolated data, and the results are directly compared with those derived from the NNR over the same time period.

3. Methodology

a. Background

As recently reviewed by Barriopedro et al. (2010b), a variety of blocking indices, differing in variables and ranging in complexity, have been used in the literature. The two most widely-used blocking indices, those proposed by Dole and Gordon (1983) and Tibaldi and Molteni (1990), are based on the 500-hPa geopotential height field. Other blocking indices use potential vorticity (Schwierz et al. 2004), stream function (Metz 1986), potential temperature on the dynamic tropopause (Pelly and Hoskins 2003) or meridional wind (Kaas and Branstator 1993). These indices also differ in the use of absolute or anomaly fields.

At present, there is no consensus on a standard or universal blocking index. This disagreement in blocking index, which is essentially caused by the different definition of blocking itself, has limited comprehensive understanding of atmospheric blocking. It is hence helpful

to critically review salient features of traditional blocking indices to better identify blocking highs. Below, the two most widely-used blocking indices applied to the 500-hPa geopotential height field and other recent approaches are briefly re-visited.

The so-called Dole-Gordon index (Dole and Gordon 1983) identifies atmospheric blocking as a persistent positive geopotential height anomaly at 500 hPa. This index provides blocking statistics on the latitude-longitude domain in a relatively simple way. It however suffers from arbitrary blocking anomaly thresholds and the need of a robust climatology to define anomalies (Doblas-Reyes et al. 2002). More importantly this approach does not necessarily detect blocking highs because persistent anomalies can be associated with weak troughs, subtropical highs or sub-polar highs which do not really block the westerly flow (Liu 1994). In spite of refinements to the Dole-Gordon index, such as more severe threshold values (e.g., Sausen et al. 1995) or defining anomalies relative to a sector mean (e.g., Mullen 1987), the possible misrepresentation still remains.

The Tibaldi-Molteni index, first introduced by Lejenas and Okland (1983) and subsequently modified by Tibaldi and Molteni (1990), is based on the reversal of the meridional gradient of 500-hPa geopotential height about a reference latitude. This index uses an absolute field, and does not suffer from thresholds for blocking anomalies. As it simply measures a local gradient about a reference latitude, it can be easily applied to any data set from operational weather forecasts to climate simulations. However the reference latitude, which prescribes the possible latitudinal locations of blocking highs, limits the detailed characterization of blocking highs (e.g., exact latitudinal location, blocking events outside of the reference regions, etc). This also hampers its application to different climate states in which preferable regions of blocking could change (Doblas-Reyes et al. 2002). These issues have been partially addressed in recent studies where the Tibaldi-Molteni index is modified to use a longitudinally-varying reference latitude or a range of latitudes (e.g., Diao et al. 2006; Scherrer et al. 2006). Despite these modifications, it retains its fundamental deficiency in identifying omega or immature blocks which are not necessarily accompanied by the reversal

of the meridional gradient over a given longitudinal range (Doblas-Reyes et al. 2002).

In the recent studies, blocking has also been examined using dynamical variables, such as potential temperature and potential vorticity in the upper troposphere or tropopause level, instead of the traditional 500-hPa geopotential height field. For instance, Pelly and Hoskins (2003) defined blocking as the reversal of the meridional gradient of potential temperature on the dynamic tropopause. Schwierz et al. (2004) used the potential vorticity anomalies integrated from 500 to 150 hPa. Alternatively, Kaas and Branstator (1993) and Cash and Lee (2000) identified blocking highs using meridional wind at 500 hPa within a region of northerly (southerly) wind upstream (downstream) at a given magnitude. These approaches are advantageous as the use of dynamical variables allows for the simultaneous identification of the regions of anomalous high pressure and strong anticyclonic circulation interrupting westerly flow. They, however, still suffer from traditional limitations such as the thresholds of the blocking anomalies and the reference latitude. The possible integration of stratospheric PV, which is not necessarily associated with blocking anomalies, is a further limiting factor in Schwierz et al. (2004).

b. A hybrid index

Barriopedro et al. (2010b) recently proposed a hybrid index by combining the Dole-Gordon and Tibaldi-Molteni indices. They first identified blocking highs by applying the Tibaldi-Molteni type index to the 500-hPa geopotential height field, and then searched for blocking anomalies around each blocked longitude as in the Dole-Gordon type index. This is essentially an extension of a 1-D blocking index (i.e., blocking frequency as a function of longitude only) to a 2-D index (i.e., blocking frequency as a function of latitude and longitude). While it better characterizes extratropical blocking highs, this index suffers from an inherently complex algorithm and a reliance on the prescribed blocking latitude.

In this study, we take a similar approach to Barriopedro et al. (2010b) but apply the Dole-Gordon index first. In other words, a contiguous area of blocking anomalies is identified

from 500-hPa geopotential height field, and then the reversal of the meridional gradient of geopotential height is evaluated about the blocking anomaly maximum. This allows us to reduce the erroneous classification of blocking by concisely implementing the meridional height reversal. In addition, the reference latitude is absent although the blocking anomaly thresholds still remain to be specified. As described below, this approach is relatively simple but more comprehensive than the traditional algorithms and can be easily applied to large data sets especially for climatological studies.

As in Barriopedro et al. (2010b), we apply our blocking index to the 500-hPa geopotential height field. The mid-tropospheric variable is useful to detect quasi-barotropic systems. It also allows us to directly compare the findings of the present study to previous results in the literature. This choice of 500-hPa geopotential height field however differs from the recent approaches that use upper-tropospheric dynamical variables which effectively detect baroclinic systems as well. While the choice of variable is still in debate and would vary depending on the purpose, Barnes et al. (2011) recently showed that most blocking events with significant amplitude and substantial spatial scale are reasonably well detected in all variables.

1) Anomalies

The geopotential height anomaly, Z', is defined as in Sausen et al. (1995) with minor modification:

$$Z' = Z - \bar{Z} - \hat{Z} \tag{1}$$

where Z is 500-hPa geopotential height normalized by the sine of latitude, $\bar{Z}$ is a running annual-mean of Z centered on a given day, $\hat{Z}$ is a mean seasonal cycle derived from Z^* which is a running-monthly mean of Z - $\bar{Z}$ centered on a given day (see Sausen et al. (1995) for further details). This treatment effectively removes the seasonal cycle and long-term variability of the background field. Note that, unlike in Sausen et al. (1995), the geopotential height

field is normalized by the sine of latitude, taking the latitudinal variation of the Coriolis parameter into account (Dole and Gordon 1983). As such Z' can be directly related with eddy streamfunction at 500 hPa in the context of quasi-geostrophic dynamics.

2) Detection

The identification and tracking algorithms of blocking highs used in this study are very similar to those in Schwierz et al. (2004). The key difference is the additional constraint for the meridional gradient reversal.

i. Blocking anomalies are first identified by the closed contours satisfying the minimum amplitude *(A)* and spatial scale *(S)*. This isolates only strong high pressure systems in synoptic scale.

ii. The blocking anomalies are then tracked in time, ensuring a sufficient overlap in blocking areas *(O)* within two days. It leaves only quasi-stationary systems.

iii. The reversal of the meridional gradient of absolute geopotential height is tested around the blocking anomalies. The height gradient is simply defined as the maximum difference of the two grid points separated by $\Delta\phi$ on the equatorward side of the blocking anomaly maximum:

$$Gr(i) = max[z(i, j^*) - z(i, j^* - \Delta\phi)] \qquad j - \Delta\phi/2 \leq j^* \leq j + \Delta\phi/2 \tag{2}$$

where z, i and j, respectively, denote 500-hPa geopotential height, the longitudinal and latitudinal locations of the anomaly maximum. The reversal is satisfied when:

$$Gr(i^*) < 0 \qquad i - \Delta\lambda/2 \leq i^* \leq i + \Delta\lambda/2 \tag{3}$$

at any longitudes within a range of $\Delta\phi$ longitudes centered about the anomaly maximum. This removes quasi-stationary ridges which do not block the zonal flow, but retains omega-shaped blocking with a weak local gradient reversal.

iv. Finally, if the above three conditions are satisfied for a consecutive period of days *(D)*, the anomaly is labelled as a blocking event.

3) Criteria

The threshold values used in this study are listed below:

i. The amplitude threshold *(A)* is set to 1.5 standard deviation of geopotential height anomalies over 30°-90°N for a 3-month period centered at a given month.

ii. The spatial-scale threshold *(S)* is set to 2.5x10^6 km^2.

iii. The overlap threshold *(O)* is 50% of area overlap in two days.

iv. The duration criteria *(D)* is set to 5 consecutive days.

v. The meridional $\Delta\phi$ and zonal $\Delta\lambda$ scales are set to 15 degrees in latitude and 10 degrees in longitude, respectively.

Among the above criteria, the blocking index is known to be particularly sensitive to the anomaly threshold value, *(A)*. In this study, we follow the standard deviation approach as in Barriopedro et al. (2010b) but with a stricter threshold of 1.5 standard deviation. This filters out relatively weak or immature blocking highs. The 1.5 standard deviation threshold further yields a seasonal cycle of NH blocking frequency in better qualitative agreement with the seasonal cycle of low-frequency (periods of 10-90 days) eddies in comparison to the seasonal cycles obtained using lower threshold values (not shown).

The remaining criteria have received only slight modifications but are generally similar to the values proposed by Schwierz et al. (2004) and Barriopedro et al. (2010b). These thresholds are less arbitrary since they largely depend on the typical scales of synoptic weather systems. Moreover, sensitivity tests have shown that the index is robust to changes in these thresholds (see appendix).

4) Impact of the height gradient reversal

As described above, a key difference between the current blocking index and the traditional Dole-Gordon type indices is the additional constraint of the height gradient reversal. The impact of this additional constraint is briefly described in this section. Figure 1a presents the 50-year climatology of the annual-mean blocking frequency derived from the NNR. The blocking climatology without the height gradient reversal is also shown in Fig. 1b. This is simply calculated by skipping the third step of the sub-section 2). It is evident that overall blocking frequency is substantially, about 25%, larger in Fig. 1b, suggesting that the height gradient reversal effectively reduces the mis-detection of quasi-stationary ridges or immature systems as blocking highs. This is particularly true for PA blockings while a similar change is observed for EA blocking further west (Fig. 1c). A similar reduction is also found in high latitude blocking. Although not shown, these results are robust to the choice of threshold value of the gradient reversal. A strong negative threshold value, $Gr(i^*) << 0$, instead of a simple gradient reversal yields results that are similar to Fig. 1a with only fewer recorded events.

The importance of the gradient reversal is further illustrated in Fig. 2 for individual blocking events. Without the gradient reversal, the index, essentially identical to the Dole-Gordon index, misidentifies a quasi-stationary ridge to be a blocking high (Fig. 2a). This quasi-stationary system does not reverse the zonal flow in comparison to the blocking event identified with a hybrid index (Fig. 2b). Figure 2b shows that the hybrid index used in this study can successfully identify omega-shaped blocking which is often not well detected by the Tibaldi-Molteni type index. The geopotential height field on the onset date, October 30th, 1971, exhibits only a weak hint of omega-shaped blocking. It has developed in next few days, forming a significant blocking high on November 5th, 1971.

4. Results

a. Blocking climatology

The annual-mean and seasonal-mean blocking frequencies, derived from 50-year long NNR, are presented in Figs. 1a and 3. They are calculated as the ratio of days a blocked area occupies each grid point to the total number of days per year. Two principal regions of blocking occurrence are evident throughout the year: the one over the northwestern Europe and eastern Atlantic (EA blockings) and the other over the North Pacific (PA blockings). They are located near the end of the Atlantic and Pacific storm tracks. The comparison between the EA and PA blockings further reveals that the EA blockings occur more frequently in a broader region than the PA blockings. In general, blocking occurs more frequently in wintertime than in summertime over both basins (Fig. 3).

These results are, at least qualitatively, in good agreement with previous findings (e.g., Dole and Gordon 1983; Tibaldi and Molteni 1990). While this is encouraging as the blocking index employed in this study is somewhat different from the traditional ones, a detailed examination reveals relatively minor but noticeable differences from the previous studies. In comparison to the blocking climatology based on the Dole-Gordon type indices (Dole and Gordon 1983; Sausen et al. 1995; Croci-Maspoli et al. 2007b), the central region of the EA blockings is extended into eastern Europe and a weak hint of a third blocking-frequency maximum is present over western Russia (around 50°E) in spring and fall, the so-called Ural blocking. Eastern confinement of the EA blockings is somewhat consistent with the blocking climatology derived from the Tibaldi-Molteni type index (Tibaldi and Molteni 1990; Pelly and Hoskins 2003; Barriopedro et al. 2010b). This is due to the effect of the height gradient reversal which reduces the potential mis-detection of blockings by the Dole-Gordon type index over the western Atlantic (Fig. 1c).

The seasonal cycle of blocking frequency is further examined in Fig. 4. It presents the daily evolution of the NH blocking frequency as a function of longitude. A number of

blocking episodes are simply counted along a given longitude band from 30°N to the pole. The resulting time series are then averaged over 50 years and slightly smoothed by applying a running monthly mean filter. Again, two preferred regions of blocking occurrence, the Pacific and the Euro-Atlantic sectors, stand out. The EA blockings are typically more frequent than the PA blockings (see the bottom panel). An exception is summer time when the PA blocking frequency is quite comparable to or even higher than the EA blocking frequency (see also JJA in Fig. 3). This peculiar seasonal cycle is consistent with recent studies (e.g., Pelly and Hoskins 2003). As discussed later, overall seasonal cycle of blocking frequency qualitatively resembles that of low-frequency variability that is defined by the 500-hPa geopotential height variance for periods of 10-90 days (compare Figs. 4a and 4b).

Overall characteristics of individual blocking events are summarized in Fig. 5. The duration distribution of all events as well as the seasonal cycles of the number of blocking events, their mean duration, and intensity are particularly presented. All statistics are based on blocking onset date: i.e., a blocking episode from January 31st to February 5th is counted as January event. It is found that the number of blocking events decrease almost exponentially as blocking duration increases (Fig. 5a). As such only few events are found with a time scale of over 10 days. In regards to blocking intensity, quantified by the maximum anomaly in an individual blocking lifecycle, winter events are generally stronger than summer events (Fig. 5b) as in previous studies (e.g., Wiedenmann et al. 2002; Diao et al. 2006). This seasonality in part results from our definition of blocking anomalies. In the present study, blocking events are chosen when local anomalies are greater than 1.5 standard deviation at a given month. Since the standard deviation varies with season, with higher values in winter but lower in summer (e.g., dashed contours in Fig. 5b), blocking intensity is anticipated to change accordingly.

The average duration and number of blocking events are further shown in Figs. 5c and d. A distinct seasonal cycle is found as in previous studies: both number of blocking events and blocking duration exhibit maxima in winter but reach their minima in summer to early

fall (e.g., Wiedenmann et al. 2002; Diao et al. 2006; Barriopedro et al. 2010b). Inter-annual variability, as denoted by grey lines, shows significant year-to-year variability with relatively stronger variability in summer. Similar analyses are also performed for the EA and PA blockings separately. Although not shown, it is found that more blocked days over the Euro-Atlantic sector than the north Pacific (Fig. 1a and 3) is mainly due to more frequent occurrence of blocking there year round. Although mean duration of EA blockings is also somewhat longer than PA blocking, essentially no difference is found especially in winter and summer (not shown).

As introduced earlier, long-lasting blockings are often associated with extratropical teleconnection patterns. Figure 6 illustrates geopotential height anomalies associated with the EA and PA blockings during the cold season. A total of 333 EA and 244 PA blocking events are used to construct the composite map. Statistically significant anomalies, tested with a two-sided students *t*-test, are observed not only at the blocking regions but also on their equatorward side and far downstream. More specifically EA blockings are accompanied by dipolar geopotential height anomalies over the Atlantic (Fig. 6a). This pattern is qualitatively similar to the one associated with the negative phase of the NAO. In contrast, PA blockings are associated with a wave-train pattern over the Pacific and North America. Although this pattern is not exactly same to the PNA, the overall pattern qualitatively resembles the negative phase of the PNA. These results are in good agreement with the previous findings (e.g., Croci-Maspoli et al. 2007a).

b. GEM model performance

With NNR blocking climatology in hand, this section evaluates the geographical location and seasonal cycle of NH blockings in the GEM model. Only 20 years, from 1987 to 2006, are examined as described in the data section. Although 20 years is relatively short, the blocking climatology derived from 20-year data is found to be similar to that from 50-year data (compare Fig. 7a with Fig. 4a). Although not shown, the results presented in

this section are also largely insensitive to the analysis period. For instance, the blocking climatology derived from the first 20-years (1960-1980) shows essentially the same result.

Figure 7 shows the longitudinal distribution of blocking occurrence for NNR, GEM model, and their difference counted from 30°N to the pole. The model captures the overall longitudinal distribution of the blockings and their seasonal variability reasonably well. Nonetheless noticeable differences are present. Most of all, the peak season of EA blocking activity is delayed from late winter to spring. This results in an overestimate of blocking frequency over the EA region during March and April (Fig. 7c). It is also found that, while blocking frequency over the Euro-Atlantic sector is generally *underestimated*, blocking frequency over the north Pacific is *overestimated* especially in the cold season. Although not shown, the blocking frequency biases shown in Fig. 7c are robust to the choice of latitude band (e.g., 10-80°N or 20-70°N) indicating that blocking biases occur mostly in the mid-latitudes (see Figs. 8c,f). Provided that climate models often underestimate blocking frequency in both basins (e.g., D'Andrea et al. 1998; Scaife et al. 2010), this result is somewhat inconsistent with previous findings. Although Matsueda et al. (2009) showed that the PA blocking frequency can be significantly overestimated in their model, it occurs only when the model is integrated with very high resolution in which high-frequency eddy feedback is likely exaggerated. However, the GEM model, evaluated in this study, has a rather coarse resolution. Here it should be noted that overestimation of modelled blocking frequency was also reported in a few previous studies. By applying the Tibaldi-Molteni blocking index to CMIP3 model output, Scaife et al. (2010) found that moderate- to low-resolution climate models could overestimate blocking frequency regionally. They attributed this bias to the mean state error rather than model resolution. This finding, the importance of the mean state, is extensively discussed in the next section.

To identify the geographical distribution of blocking occurrence in the model, the latitude-longitude distributions of blocking frequency are further illustrated in Fig. 8. Only two seasons, March-April (MA) and October-November-December-January (ONDJ), are presented

as the model shows strong biases in these seasons (Fig. 7c). As stated above, PA blocking frequency is significantly overestimated both in MA and ONDJ. This sharply contrasts with the EA blocking whose frequency is generally underestimated by the model with an enhancement over southern Europe. The result of these biases is that, during the cold season, the maximum frequency of PA blockings is somewhat higher than that of the EA blockings in the model (Fig. 8b). It is also found from Fig. 8 that preferable regions of blocking activity are slightly shifted equatorward in both basins. An eastward extension is also evident over the north Pacific. These results, which are robust to the choice of critical thresholds used in the blocking index (see appendix), suggest that the model biases, illustrated in Fig. 7c, are caused not only by inaccurate representations of blocking frequency but also by misrepresentations of blocking regions by the model. Although not shown, these biases further cause the biases in the teleconnection pattern in association with blocking highs. The PNA-like pattern associated with PA blockings (e.g., Fig. 6a) exhibits stronger amplitude than NNR with slight eastward extension. Likewise, the NAO-like pattern over the Euro-Atlantic sector (e.g., Fig. 6b) is weaker and shifted slightly eastward in the model.

Figure 9 presents the number of blocking events in the NH as a function of duration. The lifetime distribution of the modelled blockings exhibits an exponential decrease with blocking persistence (see also Fig. 5a). This is in good agreement with the NNR. While small differences are found for blocking events with a timescale of 6 to 9 days, they are statistically insignificant at the 95% level. Decomposition of the lifetime distribution by basin reveals that these differences result from a slightly larger number of PA blocking events (not shown). This result (and other results which are not presented here) suggests that the GEM model reproduces overall characteristics of individual blocking events reasonably well if they occur.

5. Possible error sources

Ascribing model biases to physical causes is difficult to achieve without systematic model experiments by varying model resolution, physical parametrizations and boundary conditions. Regardless of model configuration, however, there are general sources of error that lead to biases in low-frequency variability. For blocking highs, it is well known that misrepresentation of the time-mean flow and high-frequency eddies could be culprits of model biases in blocking frequency, intensity and duration (e.g., Barriopedro et al. 2010a; Scaife et al. 2010). As such, this section attempts to relate the model biases in blocking climatology with those in time-mean flow and transient eddies. In order to better understand overestimate of PA blocking frequency, the energetics are also briefly discussed.

a. Time-mean flow and transient eddies

Figure 10 presents stationary eddies at 500 hPa, defined by the zonally asymmetric component of the climatological geopotential height field, during ONDJ (top) and MA (bottom row) for NNR (left), GEM model (middle) and their difference (right column). It is found that stationary eddies, with primarily components of zonal wave number one (k=1) and two (k=2), are reasonably well reproduced by the model. However noticeable differences, which do not exactly mirror blocking biases shown in Figs. 8c,f, are observed over the eastern North Pacific and Euro-Atlantic regions (Figs. 10c,f). In general, the model biases are dominated by k=1 in relatively low latitudes. In high latitudes, they exhibit k=2 pattern.

A key feature of modelled stationary eddies in ONDJ is its eastward extension to the eastern Pacific and to central Russia in comparison to NNR (Figs. 10a-c), concurrent with the overall shift in blocking activity centers to the east (Figs. 8a-c). Strong negative biases are particularly evident over the central North Pacific and Northern Europe as a result of a deeper Pacific trough and a split in the Euro-Atlantic ridge. By referring to NNR, these biases project positively onto the Pacific trough but negatively onto the Euro-Atlantic ridge,

although they are slightly shifted to the east. This opposite projection is more clearly illustrated in Fig. 11a where stationary eddies are integrated from 30°N to 70°N to isolate their longitudinal structure. Decomposition of stationary eddies into k=1 and k=2 components indicates that the model biases in ONDJ are dominated by k=2 component (Fig. 11b) with an additional contribution by k=1 component from mid-October to mid-November (Fig. 11c).

The opposite projection of model biases to climatological background flow over the two basins may have important implications to model blocking biases. For instance, if blocking highs are the result of the resonant interaction between quasi-stationary and transient eddies (Nakamura et al. 1997; Cash and Lee 2000), this would provide a preferable condition for more frequent blocking over the Pacific (through stronger interaction over the deeper trough) but less frequent blocking over the Euro-Atlantic regions (through weaker interaction over the weaker ridge) in accordance with model blocking biases during ONDJ (Fig. 8c). This consistency, however, does not provide a causal relationship because biases in stationary eddies are partly caused by blocking biases themselves.

During MA, the model exhibits a significant eastward and equatorward shift in stationary eddies (Figs. 10d-f) as in blocking bias (Figs. 8d-f). This misplacement is primarily due to k=1 component around 30-50°N (Fig. 10f, 11c). It is also found that model biases largely result in a deeper than normal trough over the Pacific and higher than normal ridge over Southern Europe. In other words, in contrast to ONDJ bias, model bias in these months projects positively over the two basins. It supports the above argument: resonance interaction between quasi-stationary and transient eddies may be enhanced in the model during MA. This is again consistent with more frequent blocking activities on the equatorward side of the NNR blocking frequency maxima over the two basins. The deeper than normal Pacific trough in both seasons ONDJ and MA, is further consistent with Tyrlis and Hoskins (2008), who found that the frequency and location of PA blocking is strongly dependent on the climatological Pacific trough.

The mean-flow bias is further examined in Fig. 12 with regards to the climatological jets at 500 hPa. Although the model is able to reproduce westerly jets reasonably well, both the Pacific and Atlantic jets are somewhat overestimated at the exit regions due to the southeastward extension of the Pacific jet and to the eastward extension of the Atlantic jet in the model in both ONDJ and MA. An equatorward shift of the Pacific jet (Figs. 12b,e) may have an important implication for blocking climatology there. Specifically this may provide a preferable condition for more frequent blocking, consistent with model blocking biases. Kaas and Branstator (1993) indicated that a background flow with an equatorward-shifted jet tends to allow more frequent blocking occurrence. This contrasts with the Atlantic jet whose eastward extension would play an opposite role (Fig.12b,e). The zonally-elongated and strengthened jet weakens diffluence at the exit region of the Atlantic jet, preventing blocking formation (see the stronger meridional wind shear over northern Europe in the model, Figs. 12c,f). It should be emphasized again that all of these results could just be self-consistent as the biases in time-mean flow could simply result from those in blocking activities.

Next we examine the model biases in transient eddies. Transient eddy activities are quantified in this study by using the variance of 500-hPa geopotential height anomalies. High-frequency (period shorter than 10 days) and low-frequency eddies (10-90 days) are examined separately to highlight their difference. Figure 13 shows the longitudinal distribution of high-frequency and low-frequency eddy activities as a function of calendar day. It can be seen that low-frequency eddy activities are quite similar to those of blocking frequency (compare Figs. 7 and 13a-c). Their biases also resemble blocking biases reasonably well. For instance, Atlantic-Pacific blocking biases in ONDJ and seasonal delay in peak EA blocking frequency during MA are evident in low-frequency eddies (Fig. 13c). It is noteworthy that, unlike the blocking frequency climatology, low-frequency eddy activity is somewhat stronger over the Pacific than over the Atlantic during January-February (Figs. 13a,b). This difference is not surprising as not all low-frequency eddy activities are associated with blocking highs.

In addition, low-frequency eddy activities include information about amplitude whereas the blocking frequencies include only frequency information (although individual blockings have to satisfy an amplitude criterion).

Figures 13d-f indicate that the model successfully reproduces the seasonal cycle of both Atlantic and Pacific storm tracks. However it underestimates high-frequency eddies in all seasons and almost everywhere. This underestimate is particularly strong over the Euro-Atlantic region during ONDJ. If blocking highs are forced and maintained by high-frequency eddies (e.g., Nakamura et al. 1997), this result would provide an additional explanation for why EA blocking frequency in ONDJ is substantially underestimated although it does not explain the overestimation of PA blocking in ONDJ and the seasonal delay of EA blockings in MA. This result indicates that the role of high-frequency eddies on blocking formation and maintenance may differ with seasons and geographical locations.

b. Energetics

The above result suggests that the overestimation of PA blocking is more likely associated with biases in time-mean flow rather than high-frequency eddies. To better understand the possible impact of time-mean flow bias on PA blocking frequency, this section briefly examines energetics at 500 hPa. Note that energetics are examined to qualitatively relate the time-mean flow and low-frequency eddy activities. We are not intending to provide a complete picture of the energy cycle associated with blocking highs.

A number of studies have shown that two major sources of low-frequency eddy kinetic energy (EKE) at the exit regions of westerly jets, where blocking forms most frequently, are barotropical energy conversion (BTC) from the time-mean flow and non-linear energy transfer from high-frequency eddies to low-frequency eddies (Simmons et al. 1983; Sheng and Derome 1991a,b). For BTC, Simmons et al. (1983) have shown that the longitudinally-varying background flow plays a crucial role. Since blocking highs can be qualitatively understood by low-frequency eddy activities (Figs. 13a-c), blocking biases can be related to

time-mean flow biases by analyzing BTC below.

The barotropic energy conversion from the time-mean flow to transient eddies, is given by:

$$BTC = -(\overline{u'^2} - \overline{v'^2}) \left[\frac{1}{a\cos\phi} \frac{\partial \bar{u}}{\partial \lambda} - \bar{v} \frac{\tan\phi}{a} \right] - (\overline{u'v'}) \left[\frac{\cos\phi}{a} \frac{\partial}{\partial \phi} \left(\frac{\bar{u}}{\cos\phi} \right) + \frac{1}{\cos\phi} \frac{\partial \bar{v}}{\partial \lambda} \right] \quad (4)$$

where u and v are the zonal and meridional wind components respectively, overbars represent a time average, primes denote deviations from the time mean, λ is the longitude, ϕ is the latitude and a is the radius of the earth (Simmons et al. 1983). It is shown by Simmons et al. (1983) that the above equation can be simplified in the mid-latitudes to a good approximation to the form:

$$BTC \simeq \mathbf{E} \cdot \nabla \bar{u} = -(\overline{u'^2} - \overline{v'^2}) \frac{1}{a\cos\phi} \frac{\partial \bar{u}}{\partial \lambda} - (\overline{u'v'}) \frac{1}{a} \frac{\partial \bar{u}}{\partial \phi} \quad (5)$$

where the **E** vector is defined as in Hoskins et al. (1983) as:

$$\mathbf{E} = -(\overline{u'^2} - \overline{v'^2}, \overline{u'v'}) \quad (6)$$

The first term on the right hand side describes energy transfer due to anisotropy of the disturbances and zonally-varying background flow. Transient eddies extract KE from the mean flow when zonally elongated eddies ($\overline{u'^2} > \overline{v'^2}$) occur in the region of diffluence ($\partial \bar{u}/\partial \lambda < 0$). This contrasts with the second term on the right hand side that is the classical BTC from the zonally uniform flow to the eddies by an upgradient eddy momentum flux.

Figure 14 presents low-frequency **E**-vectors superimposed on climatological zonal wind during ONDJ and MA. Significant low-frequency eddy activities are observed at the exit regions of the westerly jets. In ONDJ, the model shows stronger westerlies over the central North Pacific and western Europe than NNR (Fig. 14c; see also Fig. 12c). This excessive zonal wind results in enhanced stretching deformation over the eastern North Pacific and reduced deformation over the central North Atlantic. Since **E**-vectors in these regions are directed westward, this background flow allows more effective BTC over the eastern North

Pacific but less effective BTC over the eastern North Atlantic. Enhanced westward **E**-vectors around the west coast of North America where westerlies decrease with longitude ($\partial\bar{u}/\partial\lambda < 0$) and near Iceland where westerlies slightly increase with longitude ($\partial\bar{u}/\partial\lambda > 0$) also likely contributed to dipolar biases in blocking frequency over the two basins. This result is consistent with blocking biases during ONDJ (Fig. 8c). A similar argument also holds for PA blocking during MA (Fig. 14d-f), although EA blocking cannot be simply explained by this.

6. Summary and Conclusions

The performance of the Global Environmental Multiscale (GEM) model is evaluated in this study in the context of the Northern Hemisphere (NH) blocking climatology. Geographical distribution, seasonal cycle and statistics of individual blocking events are quantitatively compared with those derived from the NCEP-NCAR Reanalysis (NNR). This comparison is conducted by applying a novel blocking index to the GEM and NNR data in a same resolution.

The blocking index used in this study is a hybrid index which combines the two widely-used blocking indices, namely the Dole-Gordon and Tibaldi-Molteni indices, in a simple way. Specifically blocking highs are identified by assuring the latitudinal gradient reversal in 500-hPa geopotential height field, as in the Tibaldi-Molteni type index, on the equatorward side of blocking anomalies which are defined by the Dole-Gordon type index. This approach effectively removes quasi-stationary ridges which are often mis-detected as blockings in the Dole-Gordon type index. It also allows us to detect relatively weak omega-shape blockings which are often ignored in the Tibaldi-Molteni type index.

It is found that the GEM model reproduces individual blocking events reasonably well. The total number of NH blocking events and their duration and intensity are quantitatively well simulated in comparison to the NNR. However, significant biases are found in blocking

frequency over the two basins with seasons. The biases can be summarized in three key aspects: (1) The peak season of Euro-Atlantic (EA) blocking activity is delayed from winter to early spring. (2) The EA blocking frequency is generally underestimated in the cold season. (3) The north Pacific (PA) blocking frequency is overestimated in most seasons. The last point, the overestimate of the PA blockings, is the most peculiar finding in this study as numerical models typically underestimate blocking activity over both the Euro-Atlantic and north Pacific basins (D'Andrea et al. 1998; Doblas-Reyes et al. 2002; Barriopedro et al. 2010a).

The blocking biases are found to be largely associated with the biases in the time mean flow. More specifically stationary wave activity in the model exhibits a seasonal delay and equatorward shift in zonal wavenumber one component. This is consistent with the seasonal delay in maximum EA blocking frequency and overestimated PA blocking frequency. In high latitudes, zonal wavenumber two component shows an eastward shift, yielding a deeper than normal trough over the north Pacific and shallower than normal ridge over the north Atlantic in the total stationary eddy field. This likely results in a stronger interaction between quasi-stationary waves and transient waves over the north Pacific but a weaker interaction over the north Atlantic, possibly explaining anomalous blocking activity over the two basins with opposite sign during most seasons. Although this does not provide a causal relationship as the mean-flow biases may simply result from the blocking biases themselves, a similar consistency is not found in high-frequency eddies which are underestimated over both basins in most seasons. This indicates that the possible non-linear energy transfer from high-frequency transient eddies to quasi-stationary blocking anomalies may not be a direct cause of the overestimate of PA blocking in ONDJ and MA and the seasonal delay in EA blocking in late winter, although it may play a role in cold season EA blocking which is underestimated by the model. A similar conclusion, significant blocking frequency biases by the mean flow biases, was reported in the recent study by Scaife et al. (2010) who examined a series of climate models participating in the CMIP3.

The importance of the time-mean flow in blocking biases is further supported by the energetics. It is particularly found that the model biases in PA blocking frequency are consistent with barotropic energy conversion from the mean flow to low-frequency eddies. The model shows an southeastward extension of the Pacific jet in most seasons. Westerly biases are also evident over Europe in the cold season. These biases result in stronger (weaker) stretching deformation over the north Pacific (eastern Atlantic-Europe), causing stronger (weaker) barotropic energy transfer to the low-frequency eddies there. However a corresponding energy transfer for the Euro-Atlantic sector in March and April is not clear.

The causes of time-mean flow and transient eddy biases, which are inherently linked to blocking biases as summarized above, are not addressed in this study. They could result from insufficient model resolution, unrealistic physics, prescribed (not interactive) surface boundary conditions, etc. Although this has been attempted in recent studies, e.g., by Matsueda et al. (2009) who documented the importance of model resolution in simulating EA blockings and by Scaife et al. (2011) who found an improved EA blocking simulation by prescribing more accurate SST's in the Gulf stream region, addressing these issues in the GEM model would require systematic model sensitivity tests. This is beyond the scope of the present study.

It should be stated that overall results reported here could be sensitive to the choice of blocking index. In fact, PA blocking biases become much smaller when a classical Tibaldi-Molteni index is applied. This likely results from the ignorance of omega shaped blocking in the Tibaldi-Molteni index. Likewise, if a blocking index is applied to a dynamic variable in the upper troposphere (e.g., potential vorticity on the 2 PVU surface) instead of a thermodynamic variable in the mid-troposphere as done in this study, quantitatively different results could emerge. However, given the similarity between the blocking climatology found in this study and low-frequency variability at 500 hPa (Figs. 7c and 13c), we believe that overall results would not change in quality.

Acknowledgments.

We are grateful to John Gyakum, Eyad Atallah, David Small, Jacques Derome and Stephen Colucci for their helpful discussion.

REFERENCES

Austin, J. F., 1980: The blocking of middle latitude westerly winds by planetary-waves. *Quart. J. Roy. Meteor. Soc.*, **106**, 327–350.

Barnes, E. A. and D. L. Hartmann, 2010: Influence of eddy-driven jet latitude on North Atlantic jet persistence and blocking frequency in CMIP3 integrations. *Geophys. Res. Lett.*, **37**, doi:10.1029/2010GL045700.

Barnes, E. A., J. Slingo, and T. Woollings, 2011: A methodology for the comparison of blocking climatologies across indices, models and climate scenarios. *Clim. Dynam.*, **23**, 1–15.

Barriopedro, D., R. Garcia-Herrera, J. F. Gonzalez-Rouco, and R. M. Trigo, 2010a: Application of blocking diagnosis methods to General Circulation Models. part II: model simulations. *Clim. Dynam.*, **35**, 1393–1409.

Barriopedro, D., R. Garcia-Herrera, and R. M. Trigo, 2010b: Application of blocking diagnosis methods to General Circulation Models. part I: a novel detection scheme. *Clim. Dynam.*, **35**, 1373–1391.

Cash, B. and S. Lee, 2000: Dynamical processes of block evolution. *J. Atmos. Sci.*, **57**, 3202–3218.

Colucci, S., 1985: Explosive cyclogenesis and large-scale circulation changes - implications for atmospheric blocking. *J. Atmos. Sci.*, **42**, 2701–2717.

Colucci, S. J., A. Z. Loesch, and L. F. Bosart, 1981: Spectral evolution of a blocking episode and comparison with wave interaction theory. *J. Atmos. Sci.*, **38**, 2092–2111.

Côte, J., J. Desmarais, S. Gravel, A. Methot, A. Patoine, M. Roch, and A. Staniforth, 1998a: The operational CMC-MRB Global Environmental Multiscale (GEM) model. part II: Results. *Mon. Wea. Rev.*, **126**, 1397–1418.

Côte, J., S. Gravel, A. Methot, A. Patoine, M. Roch, and A. Staniforth, 1998b: The operational CMC-MRB Global Environmental Multiscale (GEM) model. part I: Design considerations and formulation. *Mon. Wea. Rev.*, **126**, 1373–1395.

Croci-Maspoli, M., C. Schwierz, and H. C. Davies, 2007a: Atmospheric blocking: space-time links to the NAO and PNA. *Clim. Dynam.*, **29**, 713–725.

Croci-Maspoli, M., C. Schwierz, and H. C. Davies, 2007b: A multifaceted climatology of atmospheric blocking and its recent linear trend. *J. Climate*, **20**, 633–649.

D'Andrea, F., et al., 1998: Northern Hemisphere atmospheric blocking as simulated by 15 atmospheric general circulation models in the period 1979-1988. *Clim. Dynam.*, **14**, 385–407.

Diao, Y., J. Li, and D. Luo, 2006: A new blocking index and its application: Blocking action in the Northern Hemisphere. *J. Climate*, **19**, 4819–4839.

Doblas-Reyes, F., M. Casado, and M. Pastor, 2002: Sensitivity of the Northern Hemisphere blocking frequency to the detection index. *J. Geophys. Res.*, **107**, doi:10.1029/2000JD000290.

Dole, R. and N. Gordon, 1983: Persistent anomalies of the extratropical Northern Hemisphere wintertime circulation - geographical-distribution and regional persistence characteristics. *Mon. Wea. Rev.*, **111**, 1567–1586.

Dole, R., et al., 2011: Was there a basis for anticipating the 2010 Russian heat wave? *Geophys. Res. Lett.*, **38**, doi:10.1029/2010GL046582.

Egger, J., 1978: Dynamics of blocking highs. *J. Atmos. Sci.*, **35**, 1788–1801.

Hoskins, B., I. James, and G. White, 1983: The shape, propagation and mean-flow interaction of large-scale weather systems. *J. Atmos. Sci.*, **40**, 1595–1612.

Hu, Y., D. Yang, and J. Yang, 2008: Blocking systems over an aqua planet. *Geophys. Res. Lett.*, **35**, doi:10.1029/2008GL035351.

Kaas, E. and G. Branstator, 1993: The relationship between a zonal index and blocking activity. *J. Atmos. Sci.*, **50**, 3061–3077.

Kalnay, E., et al., 1996: The NCEP/NCAR 40-year reanalysis project. *Bull. Amer. Meteor. Soc.*, **77**, 437–471.

Kolstad, E. W., T. Breiteig, and A. A. Scaife, 2010: The association between stratospheric weak polar vortex events and cold air outbreaks in the Northern Hemisphere. *Quart. J. Roy. Meteor. Soc.*, **136**, 886–893.

Lejenas, H. and H. Okland, 1983: Characteristics of northern hemisphere blocking as determined from a long-time series of observational data. *Tellus*, **35**, 350–362.

Liu, Q., 1994: On the definition and persistence of blocking. *Tellus*, **46**, 286–298.

Martius, O., L. M. Polvani, and H. C. Davies, 2009: Blocking precursors to stratospheric sudden warming events. *Geophys. Res. Lett.*, **36**, doi:10.1029/2009GL038776.

Matsueda, M., 2011: Predictability of Euro-Russian blocking in summer of 2010. *Geophys. Res. Lett.*, **38**, doi:10.1029/2010GL046557.

Matsueda, M., R. Mizuta, and S. Kusunoki, 2009: Future change in wintertime atmospheric blocking simulated using a 20-km-mesh atmospheric global circulation model. *J. Geophys. Res.*, **114**, doi:10.1029/2009JD011919.

Metz, W., 1986: Transient cyclone-scale vorticity forcing of blocking highs. *J. Atmos. Sci.*, **43**, 1467–1483.

703 Mullen, S., 1987: Transient eddy forcing of blocking flows. *J. Atmos. Sci.*, **44**, 3–22.

704 Nakamura, H., M. Nakamura, and J. Anderson, 1997: The role of high- and low-frequency
705 dynamics in blocking formation. *Mon. Wea. Rev.*, **125**, 2074–2093.

706 Pelly, J. and B. Hoskins, 2003: A new perspective on blocking. *J. Atmos. Sci.*, **60**, 743–755.

707 Renwick, J. and J. Wallace, 1996: Relationships between North Pacific wintertime blocking,
708 El Nino, and the PNA pattern. *Mon. Wea. Rev.*, **124**, 2071–2076.

709 Rex, D. F., 1950: Blocking action in the middle troposphere and its effect upon regional
710 climate. part 1: An aerological study of blocking action. *Tellus*, **2**, 196–211.

711 Ringer, M., et al., 2006: The physical properties of the atmosphere in the new hadley
712 centre global environmental model (HadGEM1). part II: Aspects of variability and regional
713 climate. *J. Climate*, **19**, 1302–1326.

714 Sausen, R., W. Konig, and F. Sielman, 1995: Analysis of blocking events from observations
715 and ECHAM model simulations. *Tellus*, **47**, 421–438.

716 Scaife, A. A., T. Woollings, J. Knight, G. Martin, and T. Hinton, 2010: Atmospheric blocking
717 and mean biases in climate models. *J. Climate*, **23**, 6143–6152.

718 Scaife, A. A., et al., 2011: Improved Atlantic winter blocking in a climate model. *Geophys.*
719 *Res. Lett.*, **38**, doi:10.1029/2011GL049573.

720 Scherrer, S., M. Croci-Maspoli, C. Schwierz, and C. Appenzeller, 2006: Two-dimensional in-
721 dices of atmospheric blocking and their statistical relationship with winter climate patterns
722 in the Euro-Atlantic region. *Int. J. Climatol.*, **26**, 233–249.

723 Schwierz, C., M. Croci-Maspoli, and H. Davies, 2004: Perspicacious indicators of atmospheric
724 blocking. *Geophys. Res. Lett.*, **31**, doi:10.1029/2003GL019341.

725 Shabbar, A., J. Huang, and K. Higuchi, 2001: The relationship between the wintertime
726 north Atlantic oscillation and blocking episodes in the north Atlantic. *Int. J. Climatol.*,
727 **21**, 355–369.

728 Sheng, J. and J. Derome, 1991a: An observational study of the energy-transfer between the
729 seasonal mean flow and transient eddies. *Tellus*, **43**, 128–144.

730 Sheng, J. and J. Derome, 1991b: On the interactions among flow components in different fre-
731 quency bands in the Canadian-Climate-Center General-Circulation Model. *Atmos.-Ocean*,
732 **29**, 62–84.

733 Shutts, G., 1983: The propagation of eddies in diffluent jetstreams - eddy vorticity forcing
734 of blocking flow-fields. *Quart. J. Roy. Meteor. Soc.*, **109**, 737–761.

735 Simmons, A., J. Wallace, and G. Branstator, 1983: Barotropic wave-propagation and insta-
736 bility, and atmospheric teleconnection patterns. *J. Atmos. Sci.*, **40**, 1363–1392.

737 Tibaldi, S., F. DAndrea, E. Tosi, and E. Roeckner, 1997: Climatology of Northern Hemi-
738 sphere blocking in the ECHAM model. *Clim. Dynam.*, **13**, 649–666.

739 Tibaldi, S. and F. Molteni, 1990: On the operational predictability of blocking. *Tellus*, **42**,
740 343–365.

741 Trigo, R., I. Trigo, C. DaCamara, and T. Osborn, 2004: Climate impact of the European
742 winter blocking episodes from the NCEP/NCAR Reanalyses. *Clim. Dynam.*, **23**, 17–28.

743 Tyrlis, E. and B. J. Hoskins, 2008: The morphology of Northern Hemisphere blocking. *J.*
744 *Atmos. Sci.*, **65**, 1653–1665.

745 Wallace, J. and H. Hsu, 1985: Another look at the index cycle. *Tellus*, **37**, 478–486.

746 Webster, P. J., V. E. Toma, and H. M. Kim, 2011: Were the 2010 Pakistan floods predictable?
747 *Geophys. Res. Lett.*, **38**, doi:10.1029/2010GL046346.

748 Wiedenmann, J. M., A. R. Lupo, I. I. Mokhov, and E. A. Tikhonova, 2002: The climatology
749 of blocking anticyclones for the Northern and Southern Hemispheres: Block intensity as
750 a diagnostic. *J. Climate*, **15**, 3459–3473.

751 Woollings, T., A. Charlton-Perez, S. Ineson, A. G. Marshall, and G. Masato, 2010: Associa-
752 tions between stratospheric variability and tropospheric blocking. *J. Geophys. Res.*, **115**,
753 doi:10.1029/2009JD012742.

754 Woollings, T., B. Hoskins, M. Blackburn, and P. Berrisford, 2008: A new Rossby wave-
755 breaking interpretation of the North Atlantic Oscillation. *J. Atmos. Sci.*, **65**, 609–626.

APPENDIX

Sensitivity of blocking frequency biases to blocking index thresholds

To assess the sensitivity of our results to the choice of critical threshold values in our blocking index, Fig. 15 compares the latitude-longitude distributions of blocking frequency for NNR and the GEM model during ONDJ using: an amplitude threshold (A) of one standard deviation (e.g., Barriopedro et al. 2010a), a duration criteria (D) of 4 days (e.g., Pelly and Hoskins 2003) and an overlap threshold (O) of 70% (e.g., Schwierz et al. 2004) with all other threshold values fixed as in this study. These thresholds are found to be the most sensitive criteria used in the index. It can be seen that the model biases illustrated in Figs. 15c,f,i are in qualitative agreement with the results in Figs. 8a-c. Underestimated blocking frequency over the EA sector and overestimated blocking frequency over the PA sector are present in all three experiments despite significant differences in the magnitude of the climatological blocking frequencies. A similar consistency with Figs. 8d-f is also found during MA (not shown). These results suggest that blocking frequency biases shown in Fig. 7c and Figs. 8c,f are robust to the choice of threshold values in our blocking index.

List of Figures

15 Climatology of NH blocking frequency for (a-c) amplitude threshold of 1 standard deviation, (d-f) duration criteria of 4 days and (g-i) overlap threshold of 70% with all other criteria as in section 3b: (a,d,g) NNR, (b,e,h) GEM model and (c,f,i) their difference during ONDJ. This figure should be compared with Figs. 8a-c. Shading is in units of percent of days per season. Contour interval in (c,f,i) is 2 percent and the zero lines are omitted. Values which are statistically significant at the 95 percent confidence level using a two-tailed t-test are shaded. 52

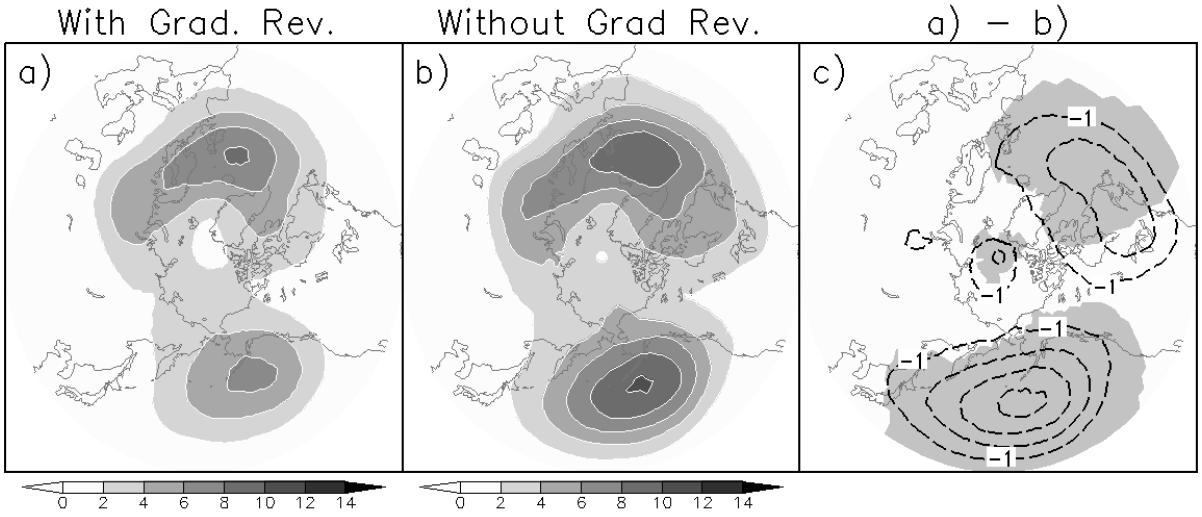

FIG. 1. Climatology of NH annual-mean blocking frequency for NNR over the period of 1960-2010: a) blocking index with height gradient reversal, b) blocking index without height gradient reversal and c) their difference. Shading interval in a) and b) is in percent of days per year. Contour interval in c) is 1 percent of days per year. Shaded areas in c) denote statistically significant differences at the 95 percent confidence level using a two-tailed student t-test.

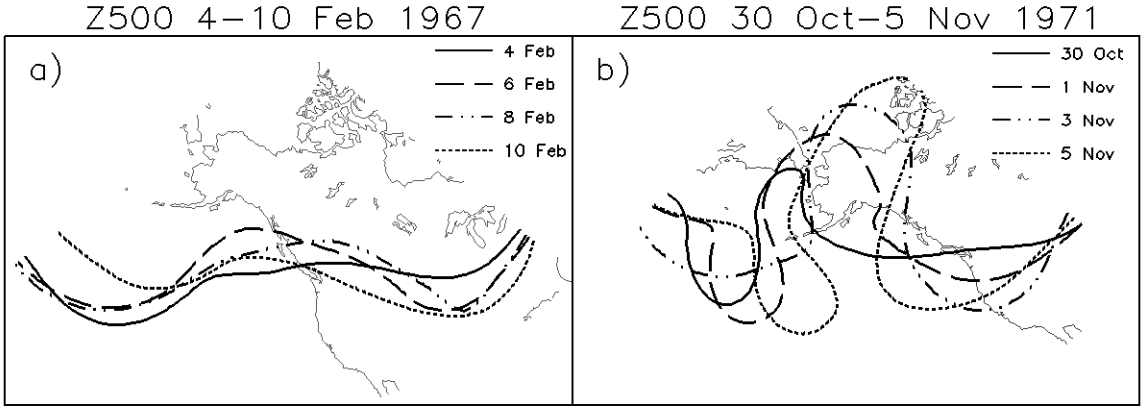

FIG. 2. Two examples of blocking events on the 500-hPa geopotential height field identified with: a) the blocking index without height gradient reversal and b) the blocking index with height gradient reversal. Contour labels show evolution in days of 5500 m contour.

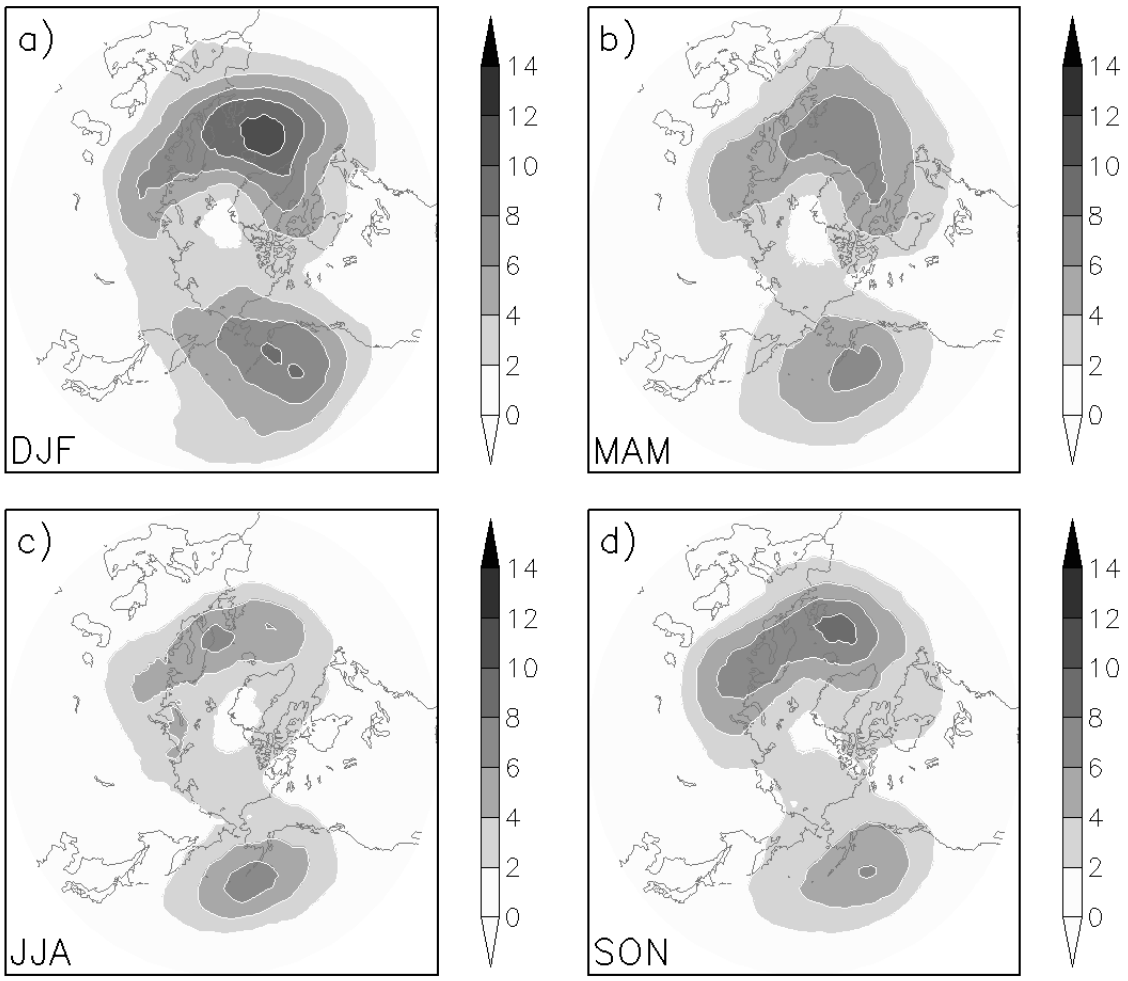

FIG. 3. Climatology of seasonal-mean NH blocking frequency from NNR over the period of 1960-2010: a) DJF, b) MAM, c) JJA and d) SON. Shading interval is in percent of days per season.

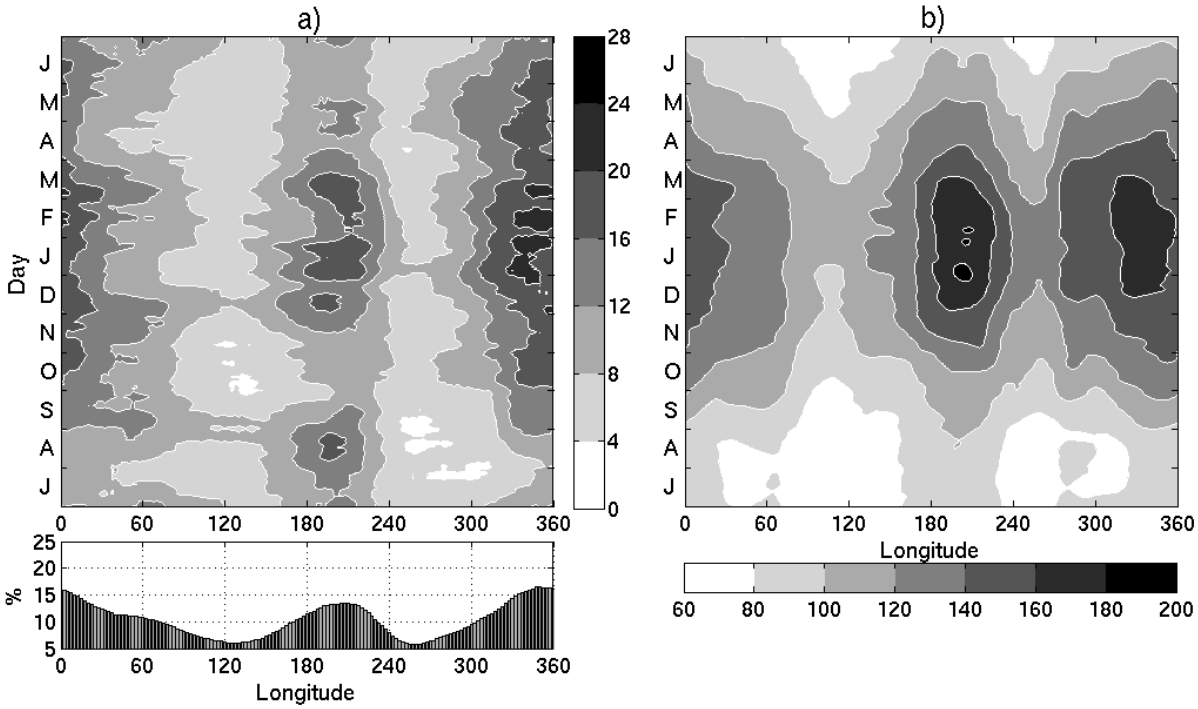

FIG. 4. (a) (top) seasonal cycle and (botttom) annual-mean of the NH blocking frequency as a function of longitude from NNR over the period of 1960-2010. Shading interval is in percent of days per 30 days centered on a given day. (b) seasonal cycle of NH low-frequency eddies from NNR. In both panels, months change from July to June.

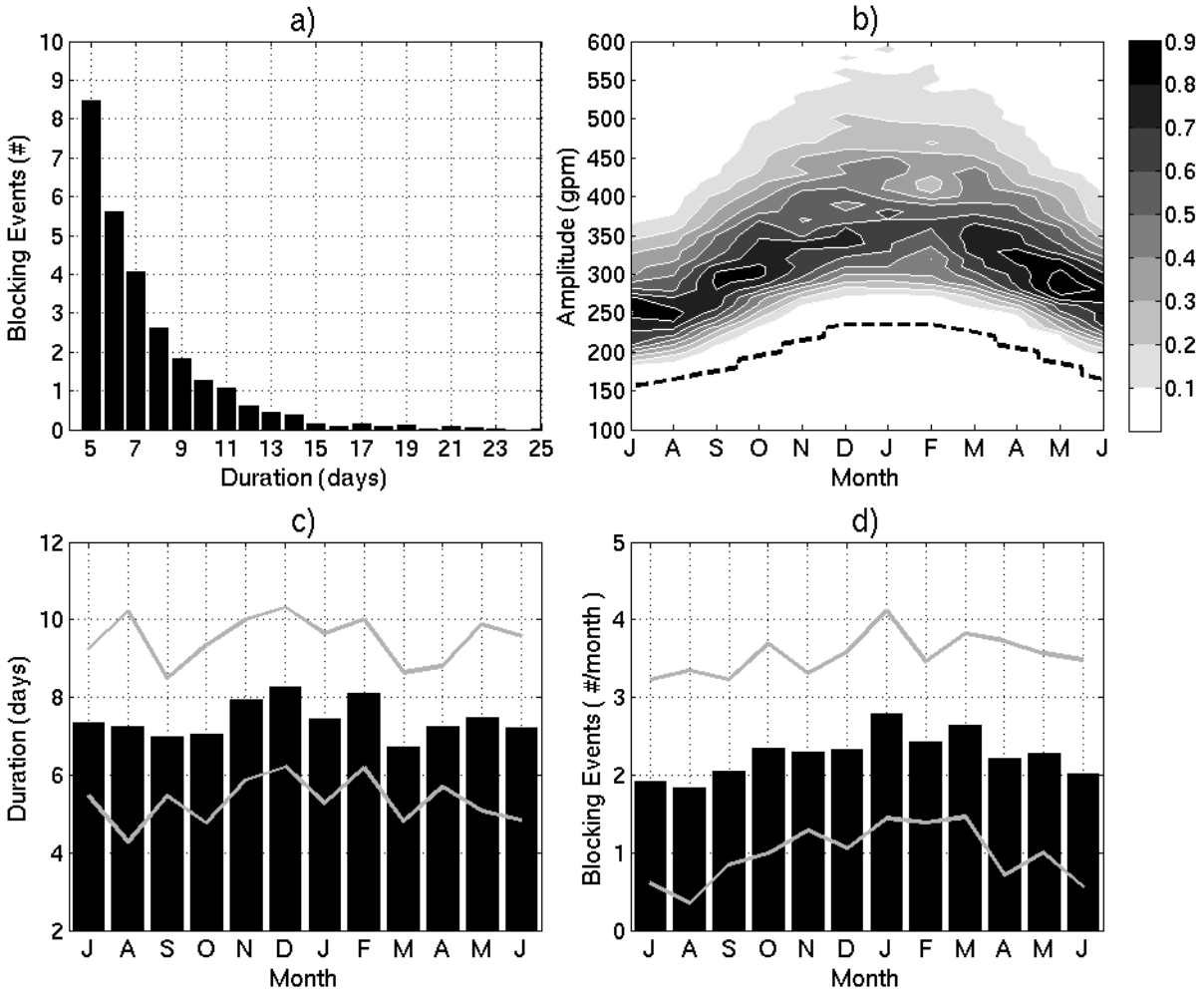

FIG. 5. Overall characteristics of individual NH blocking events from NNR for the period of 1960-2010: a) annual number of events by duration, b) number of events by intensity and month, c) duration of events by month and d) number of events by month. Dashed contours in b) represent monthly anomaly thresholds used in the blocking index. In (c,d), interannual variability, measured by one standard deviation, is shown with grey lines. In (b,c,d), the starting month is July.

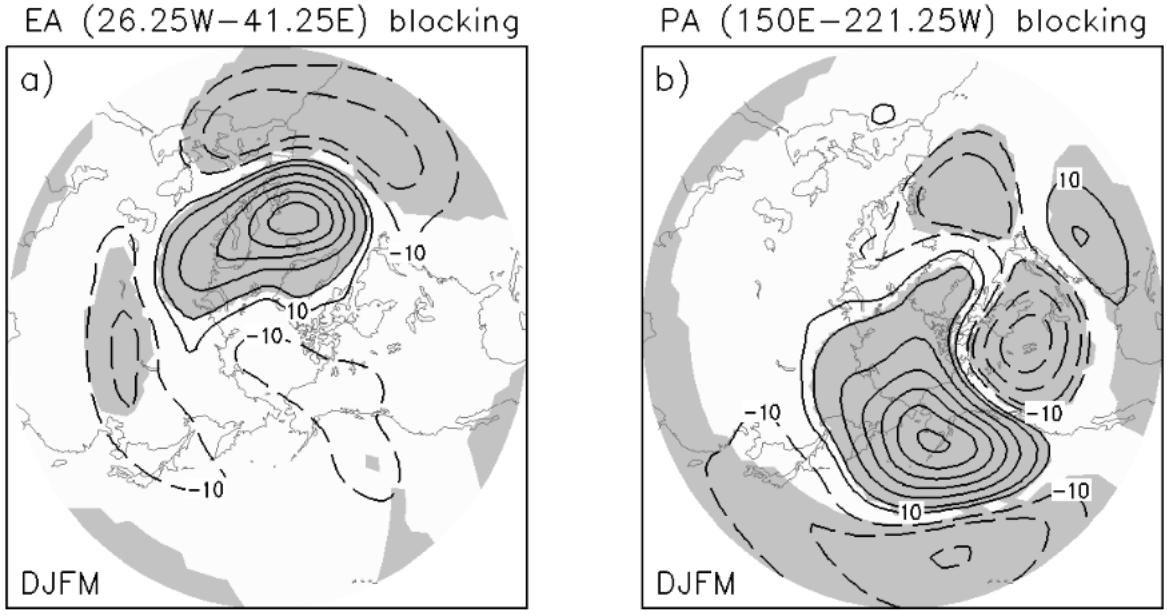

FIG. 6. DJFM 500-hPa geopotential height anomalies associated with a) EA blocking and b) PA blocking events for 50-year long NNR (1960-2010). Contour interval is 10 m and the zero lines are omitted. Shading denotes anomalies which are significantly different from zero at the 95 percent confidence level using a two-tailed student t-test.

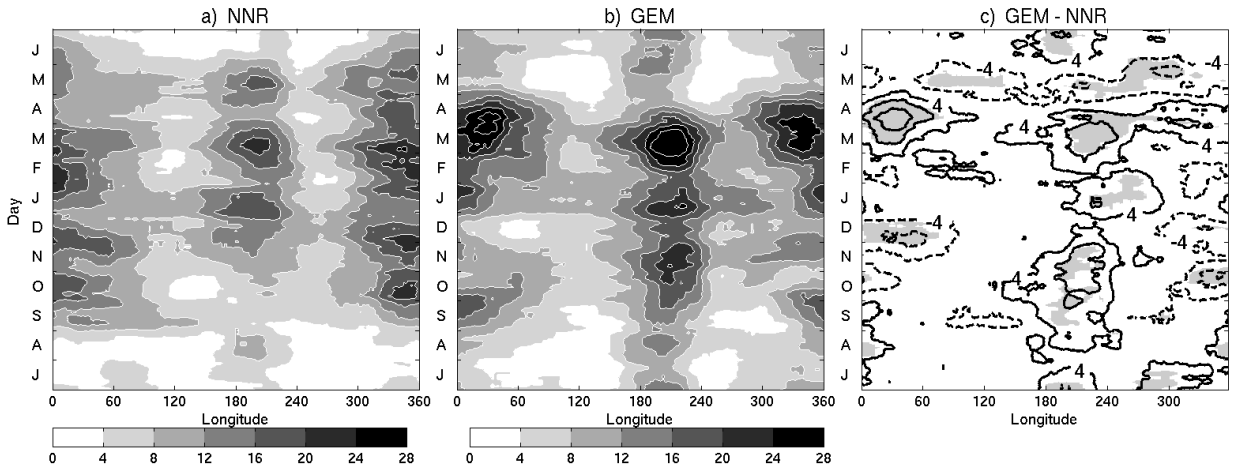

FIG. 7. Seasonal cycles of NH blocking frequency for the period of 1987-2006: a) NNR, b) model and c) their difference. Shading interval is 4 percent of days per 30 days centered on a given day. Contour interval in c) is 4 percent and the zero lines are ommited. Values which are statistically significant at the 95 percent confidence level are shaded. In all panels, months change from July to June.

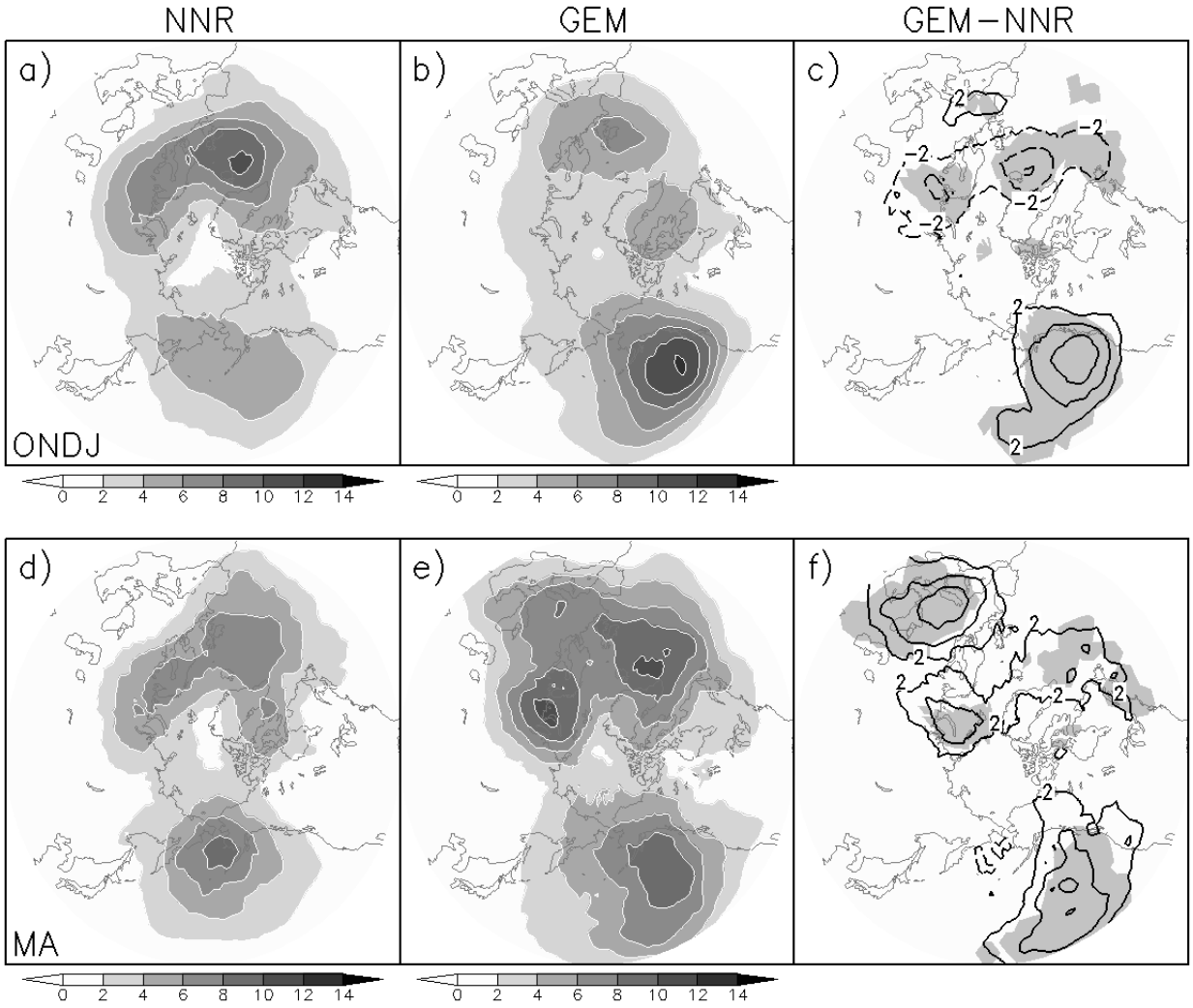

FIG. 8. Climatology of NH blocking frequency for the period of 1987-2006: (a,d) NNR, (b,e) GEM model and (c,f) their difference during (a-c) ONDJ and (d-f) MA. Shading is in units of percent of days per season. Contour interval in (c,f) is 2 percent and the zero lines are omitted. Values which are statistically significant at the 95 percent confidence level using a two-tailed t-test are shaded.

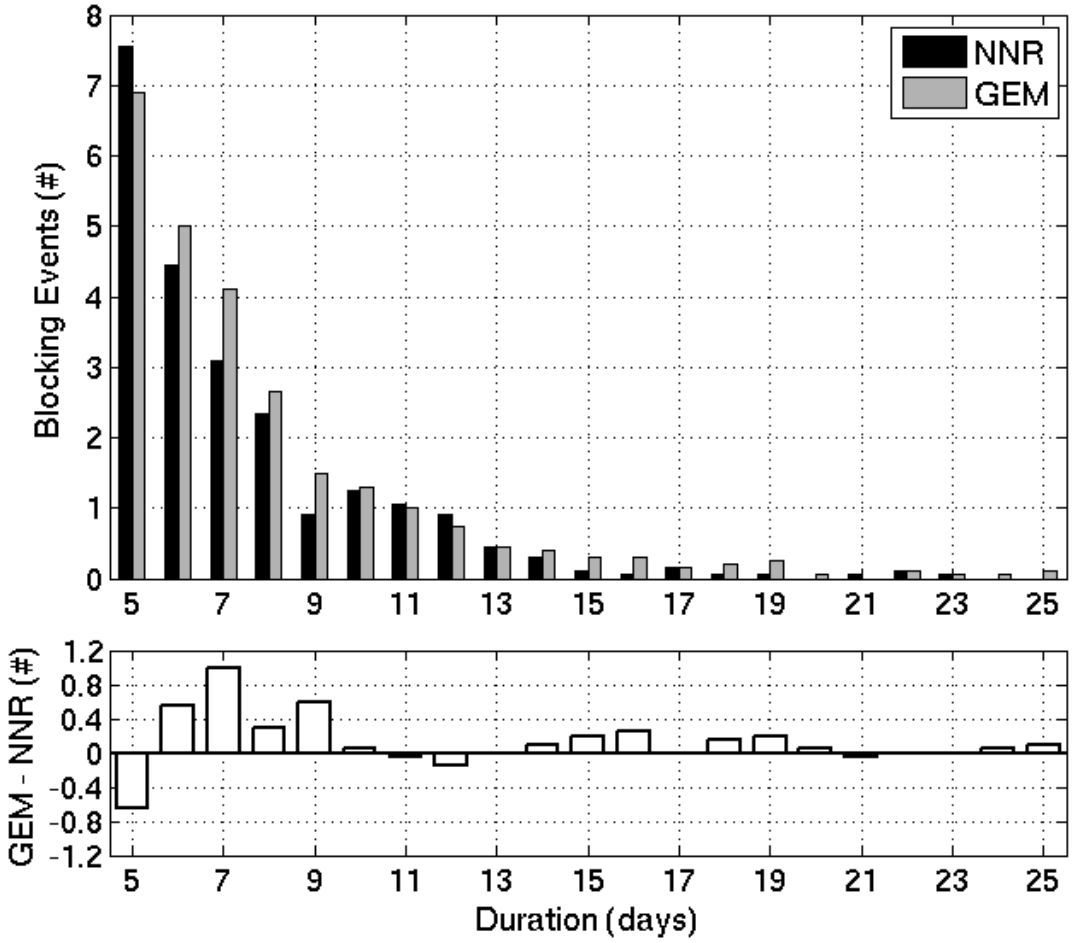

FIG. 9. Number of blocking events as a function of duration for NNR (black) and model (grey bars), and their difference for the period of 1987-2006.

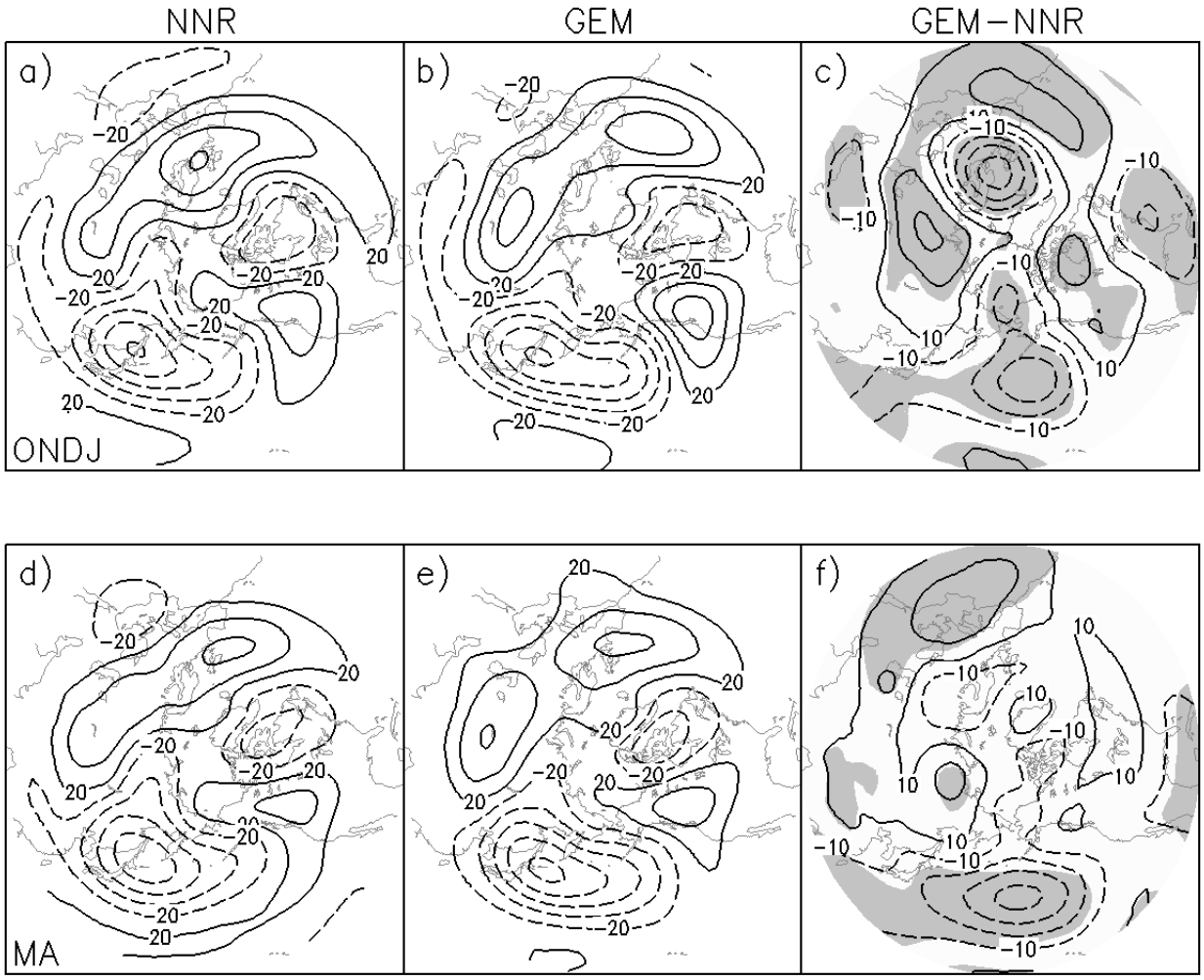

FIG. 10. Stationary eddies for (a,d) NNR, (b,e) GEM model and (c,f) their difference during (a-c) ONDJ and (d-f) MA for the period of 1987-2006. Contour interval in (a,b,d,e) is 20 m. Contour in (c,f) is 10 m and values which are statistically significant at the 95 percent confidence level are shaded. Zero lines are omitted in all figures.

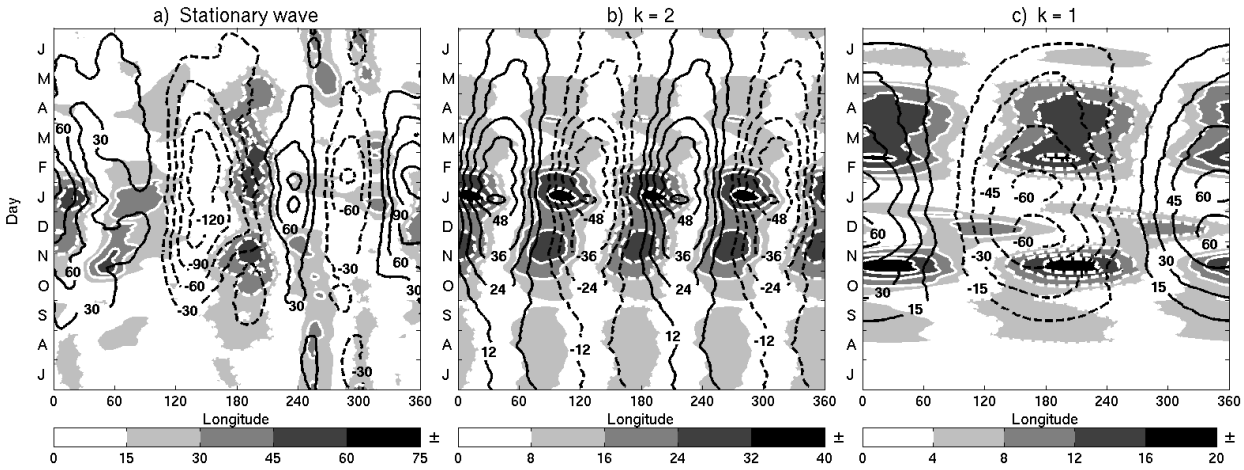

FIG. 11. Seasonal cycles of stationary eddies integrated from 30°-70°N over the period of 1987-2006: a) full, b) k=2 and c) k=1 components. NNR climatology is contoured and model biases (GEM-NNR) are shaded in grey. Positive and negative biases are denoted with solid and dashed white contours, respectively. Zero lines are ommitted in all figures. Note that shading and contour intervals are different in each panel. In all panels, months change from July to June.

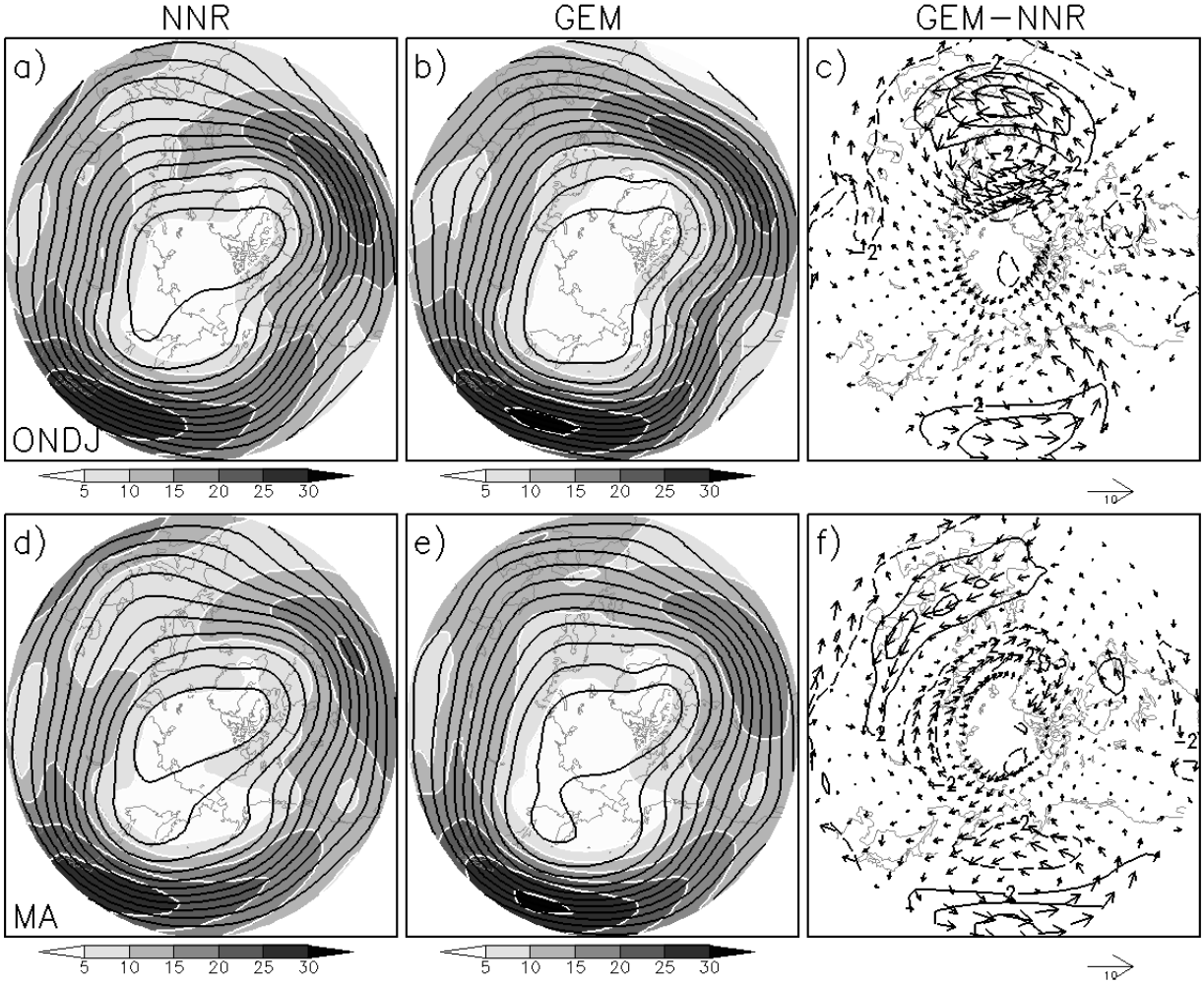

FIG. 12. Climatology of NH zonal wind (shading), streamfunction (contours) and wind vector at 500 hPa for (a,d) NNR, (b,e) GEM model and (c,f) their difference during (a-c) ONDJ and (d-f) MA for the period of 1987-2006. Stream function contour interval is 10^6 m^2s^{-1} in (a,b,d,e). Zonal wind contour interval in (c,f) is 2 ms^{-1}.

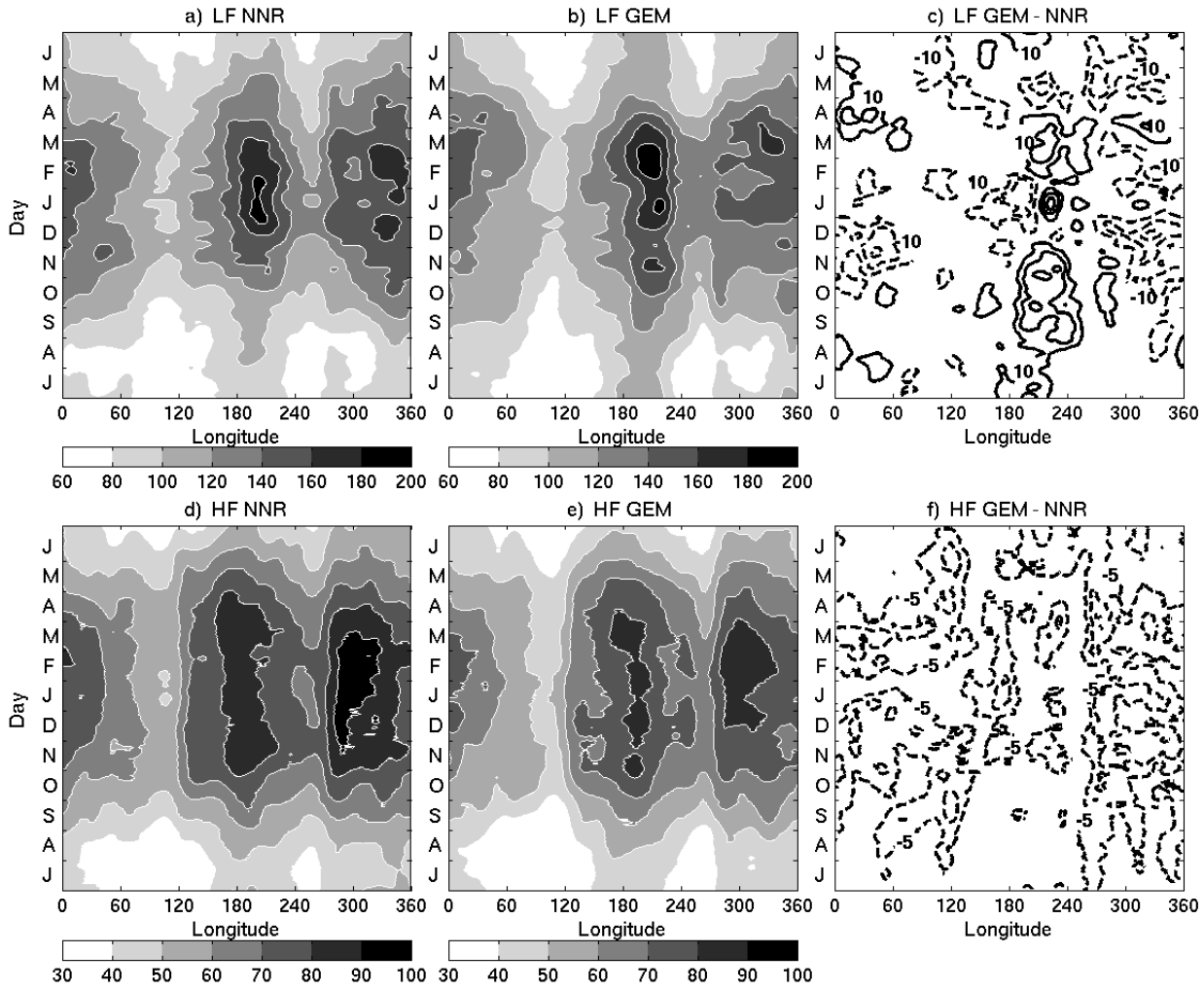

FIG. 13. Seasonal cycles of (a-c) low-frequency (LF, 10-90 days) and (d-f) high-frequency (HF, less than 10 days) eddies for (a,d) NNR, (b,e) GEM model and (c,f) their difference for the period of 1987-2006. Contour intervals in (c,f) are 10 m and 5 m respectively. Zero lines are ommitted. In all panels, months change from July to June.

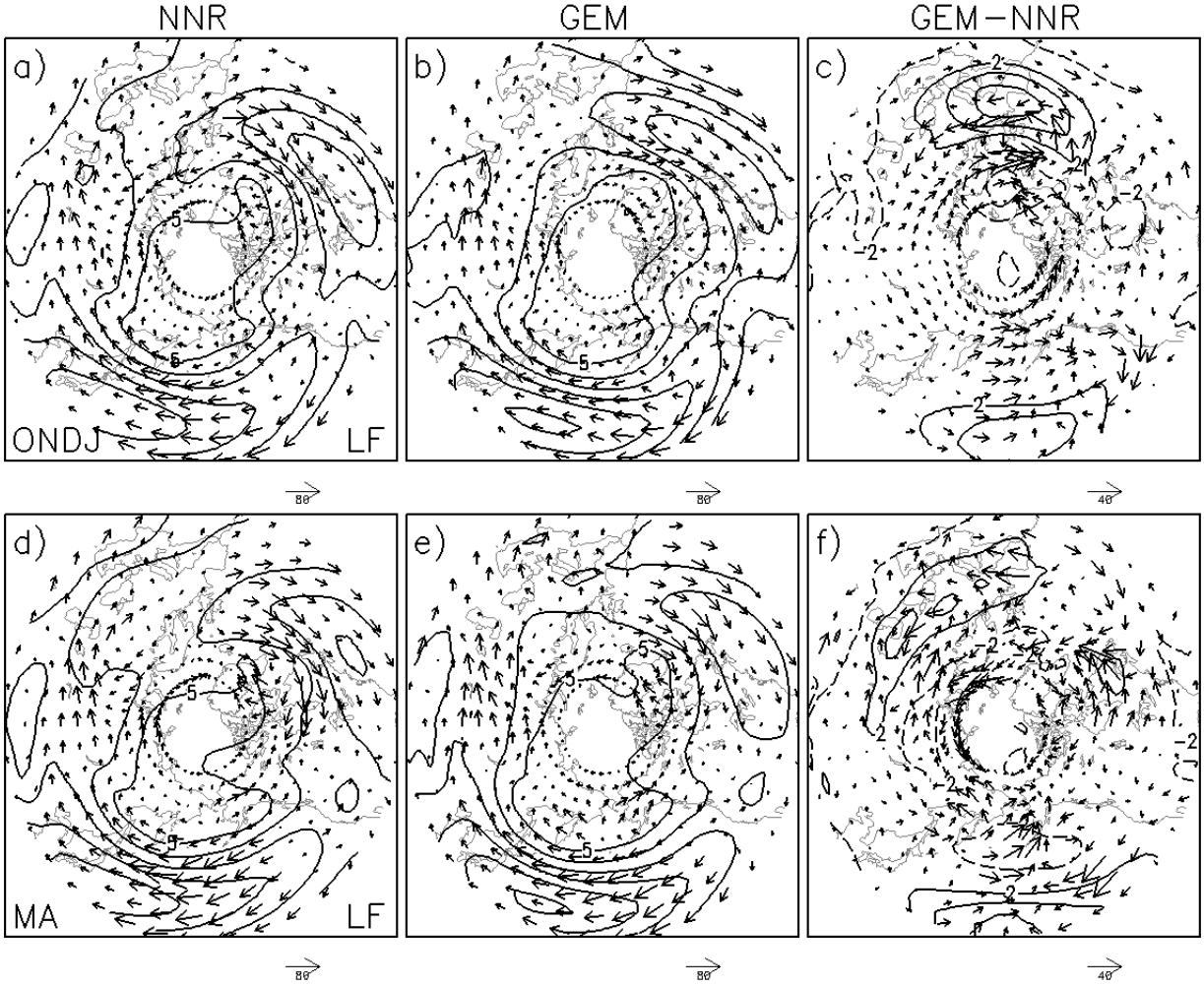

FIG. 14. Climatological zonal wind (contours) and low-frequency E-vectors for (a,d) NNR, (b,e) GEM model and (c,f) their difference during (a-c) ONDJ and (d-f) MA for the period of 1987-2006. Contour interval in (a,b,d,e) is 5 m s^{-1}. Contour interval in (c,f) is 2 ms^{-1}. Zero lines are ommitted.

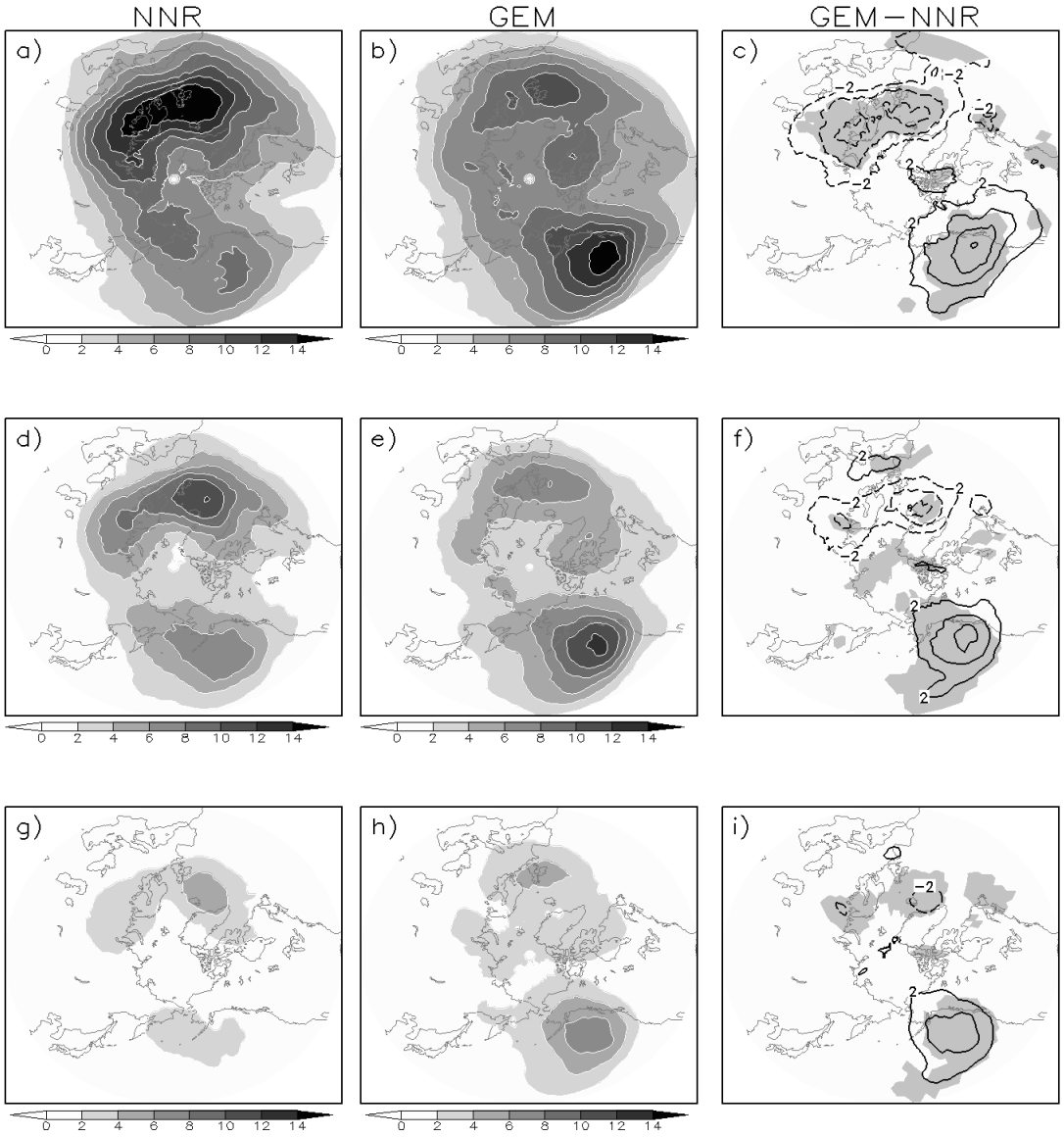

FIG. 15. Climatology of NH blocking frequency for (a-c) amplitude threshold of 1 standard deviation, (d-f) duration criteria of 4 days and (g-i) overlap threshold of 70% with all other criteria as in section 3b: (a,d,g) NNR, (b,e,h) GEM model and (c,f,i) their difference during ONDJ. This figure should be compared with Figs. 8a-c. Shading is in units of percent of days per season. Contour interval in (c,f,i) is 2 percent and the zero lines are omitted. Values which are statistically significant at the 95 percent confidence level using a two-tailed t-test are shaded.